18

Cloud thermodynamics and dynamics

Clouds affect the atmosphere in several ways. They absorb and reflect radiation, modify local air temperatures, pressures, and winds, produce precipitation, mix and remove gases and particles, and alter photolysis coefficients. In this chapter, the thermodynamics and microphysics of clouds are discussed. The thermodynamic energy equation and the vertical momentum equation for a cloud are first derived. Cumulus parameterizations for simulating effects of subgrid scale clouds in a model are then described. Finally, numerical techniques for size-resolved liquid and ice cloud microphysics are given. The techniques include those for growth of water vapor onto aerosol particles to form liquid drops and ice crystals, hydrometeor–hydrometeor coagulation, breakup of large liquid drops, contact freezing, heterogeneous/homogeneous freezing, evaporation/sublimation, evaporative freezing, ice crystal melting, and aerosol–hydrometeor coagulation. Finally, numerical methods of treating removal of aerosol particles by rainout and washout and of treating lightning generation are given.

18.1 FOG AND CLOUD TYPES AND FORMATION MECHANISMS

Clouds are a type of hydrometeor. A **hydrometeor** is an ensemble of liquid or solid water particles suspended in or falling through the air. In this section, cloud types and their formation mechanisms are described. Additional discussions of clouds can be found in Cotton and Anthes (1989), Rogers and Yau (1989), and Houze (1993).

18.1.1 Cloud classification

Clouds form primarily in the troposphere. In the tropics, the highest clouds reach heights of 18 km. In midlatitudes and at the poles, tropospheric clouds reach maximum heights of 13 and 8 km, respectively. Water ice and nitric acid ice clouds can form in the polar stratosphere. These clouds are discussed in Chapter 11. For purposes of cloud classification, the troposphere is divided into three altitude ranges or **étages**, in which clouds of different types (genera) form most frequently. These étages encompass high, middle, and low altitude ranges, as shown in Table 18.1.

In 1802, Jean Baptiste Lamarck (1744–1829) proposed a cloud classification scheme, but the cloud types he suggested were not generally accepted. In 1803,

Table 18.1 Altitude range of cloud étages

	Range (km)		
Étage	**Polar regions**	**Temperate regions**	**Tropical regions**
High	3–8	5–13	6–9
Middle	2–4	2–7	2–8
Low	0–2	0–2	0–2

Source: WMO (1975).

Luke Howard proposed an alternative identification scheme that used Latin roots in the cloud names. Sheetlike clouds were called **stratus** (Latin for *layer*). Puffy clouds were called **cumulus** (*heap*), featherlike clouds were called **cirrus** (*curl of hair*), and rain clouds were called **nimbus** (*violent rain*).

Cloud types are now categorized by 10 **genera**. Table 18.2 describes the genera and identifies the étage(s) in which each genus is most commonly observed. A given cloud belongs to one genus only.

A **fog** is essentially a cloud touching the ground, but a fog is not classified as a cloud. Instead, it has its own classification and is defined as a suspension of liquid water drops that causes visibility to be reduced to less than 1 km (WMO 1975). If visibility is greater than 1 km, the fog is called a **mist**. If the fog contains ice crystals instead of liquid water, it is an **ice fog**.

Other hydrometeors suspended in the air include rain, supercooled rain, drizzle, supercooled drizzle, snow, snow grains, snow pellets, diamond dust, hail, small hail, ice pellets, drifting snow, blowing snow, and spray. **Rain** is precipitation of water drops falling from a cloud. **Supercooled rain** is liquid rain at a temperature below 0 °C. **Drizzle** is precipitation of water drops with diameter <0.5 mm. **Supercooled drizzle** is liquid drizzle at a temperature below 0 °C. **Snow** is precipitation from a cloud of single or agglomerated ice crystals. **Snow grains** are opaque ice crystals of diameter <1 mm. **Snow pellets** are rounded white and opaque ice particles with diameters up to 5 mm. **Diamond dust** is precipitation of small ice crystals from the clear sky. **Hail** is precipitation of clumpy, spheroidal ice particles 5–50 mm in diameter. **Small hail** is precipitation of translucent, spherical ice particles near 5 mm in diameter. **Ice pellets** are transparent ice particles, either spheroidal or irregular, with diameter <5 mm.

Hydrometeors affixed to a surface include fog deposits, dew, frozen dew, hoar frost, rime, glaze, and freezing rain. **Fog deposits** are fog drops fixed to a surface when the surface temperature exceeds 0 °C. **Dew** is liquid water on a surface produced from condensation of water vapor. **Frozen dew** forms from dew if the temperature drops below 0 °C. **Hoar frost** or **frost** is ice produced by sublimation of water vapor on a surface. **Rime** is ice produced by the freezing of supercooled fog droplets on a surface when the surface temperature is below 0 °C. **Glaze** is transparent ice that forms when supercooled drizzle or rain freezes on contact with a surface. **Freezing rain** occurs when nonsupercooled drizzle or rain freezes on contact with a surface.

Table 18.2 Cloud classification

Genera	Description	Étage
Cirrus (Ci)	Detached with white, delicate filaments, whitish patches, or narrow bands. Fibrous appearance and/or silky sheen.	High
Cirrocumulus (Cc)	Thin, white patch, sheet, or layer cloud, made of small elements with grains or ripples, merged or separate, but regularly arranged.	High
Cirrostratus (Cs)	Transparent, whitish cloud veil. Fibrous or smooth, totally or partly covering the sky. Produces a halo.	High
Altocumulus (Ac)	White and/or gray patch, sheet, or layer, generally with shading. Contains rounded masses, sometimes fibrous, which may or may not be merged.	Middle
Altostratus (As)	Grayish sheet or layer, fibrous or uniform, totally or partly covers the sky. Has parts thin enough to reveal the Sun vaguely. No halo.	Middle High
Nimbostratus (Ns)	Gray, often dark. Contains rain that almost always reaches the ground. Thick enough to block the Sun. Low, ragged clouds appear below the cloud.	Low Middle High
Stratocumulus (Sc)	Gray and/or whitish, patch, sheet, or layer. Almost always has dark parts and rolls, which may or may not be merged.	Low
Stratus (St)	Gray cloud layer with uniform base that may produce drizzle, ice, or snow. When the Sun is visible through the cloud, its outline is clear. Stratus does not produce a halo, except at low temperatures.	Low
Cumulus (Cu)	Detached clouds, usually dense, with sharp outlines. Vertically developed as a rising mound, dome, or tower, of which the upper part often looks like a cauliflower. The sunlit portion appears white. Its base is dark and horizontal.	Low Middle
Cumulonimbus (Cb)	Heavy, dense cloud with great vertical extent, in the form of a mountain or tower. Part of upper cloud is smooth, fibrous, or striated, and almost always flattened, spreading out like an anvil. Under its dark base, precipitation occurs.	Low Middle High

Source: WMO (1975).

18.1.2 Cloud formation

Clouds form by one of several mechanisms. Clouds that form by surface heating and free convection are **convective clouds**. When the ground is exposed to intense sunlight, air immediately above the ground heats by conduction. The resulting unstable temperature profile causes buoyancy and lifting (free convection). The altitude at which lifting by free convection starts is the **level of free convection** (LFC). As warm air near the surface rises, it expands and cools dry-adiabatically. If the buoyant parcel contains water vapor, and if the parcel temperature cools to the **isentropic condensation temperature** (ICT), the vapor condenses, forming a cloud base. The altitude of the cloud base is the **lifting condensation level** (LCL). Release

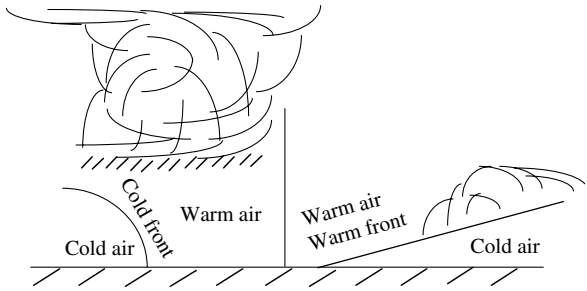

Figure 18.1 Formation of clouds along a cold and a warm front. The cold air behind a cold front forces warm air vertically. The warm air behind a warm front slides up over cold air ahead of the front. In both cases, the rising air cools and may result in cloud formation.

of latent heat during condensation at the cloud base provides buoyancy for further lifting, cooling, and cloud development.

Orographic clouds appear when a horizontal wind encounters a topographic barrier, such as a mountain, which forces the wind to shift slantwise or vertically (orographic uplifting). As the air rises, it expands and cools adiabatically. If the parcel rises to the LCL, a cloud forms.

Clouds can also form when winds converge horizontally, such as around a center of a low pressure. Convergence forces air to rise vertically (forced convection). Again, as the air rises, it expands and cools, eventually forming a cloud.

Clouds also form along weather fronts, as shown in Fig. 18.1. Along a **cold front**, cold, dense air pushes warm, moist air vertically, causing the warm air to expand and cool until condensation occurs. Along a **warm front**, warm, moist air slides over cold air and expands and cools until a cloud forms. The types of clouds that form along a cold front differ from those that form along a warm front. Ahead of a cold front, cumulonimbus, altocumulus, cirrostratus, and cirrus are the most prevalent cloud types. In front of a warm front, stratocumulus, stratus, nimbostratus, altostratus, cirrostratus, and cirrus are the most likely clouds to form.

Atmospheric stability above the LCL affects cloud type. If a cloud base is below 2 km, and the air is stable above the LCL, the cloud that forms is a cumulus humilis (cumulus cloud of slight vertical extent), stratus, or stratocumulus. If the atmosphere is unstable up to the tropopause, the cloud that forms is a cumulonimbus. Some cloud types form from interactions between other cloud types and the environment. When the top of a cirrostratus, altostratus, or stratus cloud cools and the bottom warms radiatively, the resulting buoyant motions within the cloud produce pockets of air that rise or sink to form cirrocumulus, altocumulus, or stratocumulus clouds, respectively. Cirrus clouds often form as the top of a cumulonimbus cloud dissipates.

18.1.3 Fog formation

Fogs form in one of several ways. A **radiation fog** forms when air near the ground cools radiatively during the night to the dew point. An **advection fog**, which generally appears near the coast, forms when the wind advects warm, moist air (usually ocean air) over a cold surface, cooling the air to the dew point. An **upslope fog** forms when warm, moist air flows up a topographical barrier and cools adiabatically to the dew point. The formation of this type of fog is similar to the formation of an orographic cloud. An **evaporation fog** forms when warm water evaporates and the vapor recondenses when it mixes with cool, dry air. Two types of evaporation fogs are steam fogs and frontal fogs. A **steam fog** occurs when warm surface water (e.g., from a lake or the ocean) evaporates and the vapor recondenses as it rises into cooler air, giving the appearance of rising steam. A **frontal fog** occurs when warm raindrops evaporate as they fall through a cold air mass and the vapor recondenses in the cold air. These conditions often exist ahead of an approaching front.

Fogs generally burn off from the top and bottom simultaneously. Solar energy evaporates drops at the fog top, and thermal-infrared energy emitted by the ground evaporates drops at the fog base. When the fog no longer touches the ground, it is a stratus cloud.

18.2 MOIST ADIABATIC AND PSEUDOADIABATIC PROCESSES

The extent to which a cloud grows vertically depends on atmospheric stability and moisture. In Chapter 2, stability in unsaturated air was discussed. Here, the concept of stability is extended to saturated air.

An unsaturated parcel of air rising dry-adiabatically cools at the rate of -9.8 K km^{-1}. If condensation occurs as the parcel rises, latent heat is released, offsetting the dry-adiabatic cooling, typically by $+4$ K km^{-1} but by up to $+8$ K km^{-1} in the tropics. When the released latent heat is absorbed by dry air, water vapor, and liquid water, the process is **moist adiabatic**. When, by assumption, it is absorbed by only dry air and water vapor, the process is **pseudoadiabatic**.

18.2.1 Pseudoadiabatic lapse rate

In this subsection, the pseudoadiabatic lapse-rate equation is derived. During a pseudoadiabatic ascent, the latent heat per unit mass of air (J kg^{-1}) released during condensation is

$$\mathrm{d}Q = -L_e \, \mathrm{d}\omega_{v,s} \tag{18.1}$$

where L_e is the latent heat of evaporation (J kg^{-1}) from (2.53), and $\omega_{v,s} = \varepsilon p_{v,s}/p_d$ is the mass mixing ratio (kilograms of vapor per kilogram of dry air) of water vapor at saturation over a liquid surface, defined in (2.67). Combining (18.1) with

the first law of thermodynamics from (2.87) yields

$$-L_e\,d\omega_{v,s} = c_{p,m}\,dT - \alpha_a\,dp_a \tag{18.2}$$

Substituting $\alpha_a = 1/\rho_a = R_m T/p_a$ from (2.36) into (18.2) and rearranging give

$$dT = \frac{R_m T}{c_{p,m} p_a} dp_a - \frac{L_e}{c_{p,m}} d\omega_{v,s} \tag{18.3}$$

Differentiating (18.3) with respect to altitude and combining the result with $\partial p_a/\partial z = -\rho_a g$ and $p_a = \rho_a R_m T$ yield

$$\left(\frac{\partial T}{\partial z}\right)_w = \frac{R_m T}{c_{p,m} p_a}\frac{\partial p_a}{\partial z} - \frac{L_e}{c_{p,m}}\frac{\partial \omega_{v,s}}{\partial z} = -\frac{g}{c_{p,m}} - \frac{L_e}{c_{p,m}}\frac{\partial \omega_{v,s}}{\partial z} \tag{18.4}$$

where subscript w signifies pseudoadiabatic. Equation (18.4) simplifies to (2.90), the equation for the dry adiabatic lapse rate, when $\partial\omega_{v,s}/\partial z = 0$. Differentiating $\omega_{v,s} = \varepsilon p_{v,s}/p_d$ with respect to altitude, then substituting $dp_{v,s} = L_e p_{v,s}\,dT/R_v T^2$ (Clausius–Clapeyron equation), $\omega_{v,s} = \varepsilon p_{v,s}/p_d$, $R' = \varepsilon R_v$, and $\partial p_d/\partial z = -p_d g/R'T$ yield

$$\frac{\partial \omega_{v,s}}{\partial z} = \frac{\varepsilon}{p_d}\left(\frac{\partial p_{v,s}}{\partial z} - \frac{p_{v,s}}{p_d}\frac{\partial p_d}{\partial z}\right) = \frac{L_e \varepsilon \omega_{v,s}}{R'T^2}\frac{\partial T}{\partial z} + \frac{\omega_{v,s} g}{R'T} \tag{18.5}$$

Substituting (18.5) and $\Gamma_{d,m} = g/c_{p,m}$ from (2.90) into (18.4) and rearranging give the **pseudoadiabatic temperature change with altitude** as

$$\left(\frac{\partial T}{\partial z}\right)_w = -\Gamma_w = -\Gamma_{d,m}\left(1 + \frac{L_e \omega_{v,s}}{R'T}\right)\Big/\left(1 + \frac{L_e^2 \varepsilon \omega_{v,s}}{R' c_{p,m} T^2}\right) \tag{18.6}$$

where Γ_w is the **pseudoadiabatic lapse rate** (K km^{-1}).

Example 18.1

Find Γ_w if $p_d = 950$ hPa and (a) $T = 283$ K; (b) $T = 293$ K.

SOLUTION

(a) From (2.62), $p_{v,s} = 12.27$ hPa; from (2.67), $\omega_{v,s} = 0.00803$ kg kg^{-1}; from (2.80), $c_{p,m} = 1011.6$ J kg^{-1} K^{-1} (assuming the air is saturated with water vapor); from (2.54), $L_e = 2.4761 \times 10^6$ J kg^{-1}; and from (18.6) $\Gamma_w = 5.21$ K km^{-1}.

(b) When $T = 293$ K, $p_{v,s} = 23.37$ hPa, $\omega_{v,s} = 0.0153$ kg kg^{-1}, $c_{p,m} = 1017.9$ J kg^{-1} K^{-1}, $L_e = 2.4522 \times 10^6$ J kg^{-1}, and $\Gamma_w = 4.27$ K km^{-1}. Thus, the pseudoadiabatic lapse rate changes with temperature and pressure.

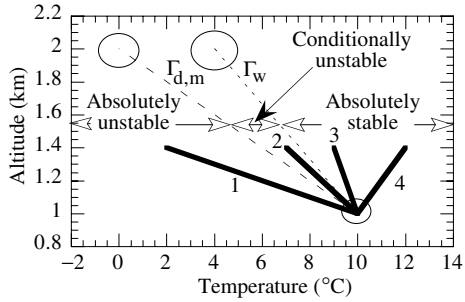

Figure 18.2 Stability criteria for unsaturated and saturated air. If air is saturated, the environmental temperature profile (thick solid lines) is compared with the pseudoadiabatic profile (right dashed line) to determine stability. Environmental temperature profiles 3 and 4 are stable and 1 and 2 are unstable with respect to saturated air. Profiles 2, 3, and 4 are stable and 1 is unstable with respect to unsaturated air. A rising or sinking air parcel follows the $\Gamma_{d,m}$-line when the air is unsaturated and the Γ_w-line when the air is saturated.

18.2.2 Stability criteria

In (2.100), stability criteria were given for unsaturated air. These criteria can be expanded to account for saturated and unsaturated air with

$$\begin{cases} \Gamma_e > \Gamma_{d,m} & \text{absolutely unstable} \\ \Gamma_e = \Gamma_{d,m} & \text{unsaturated neutral} \\ \Gamma_{d,m} > \Gamma_e > \Gamma_w & \text{conditionally unstable} \\ \Gamma_e = \Gamma_w & \text{saturated neutral} \\ \Gamma_e < \Gamma_w & \text{absolutely stable} \end{cases} \tag{18.7}$$

where $\Gamma_e = -\partial T/\partial z$ is the environmental lapse rate from Section 2.6.2.1. If, for example, $\Gamma_w = +6.0$ K km^{-1} and $\Gamma_e = +8.0$ K km^{-1} (and $\Gamma_{d,m} = 9.8$ K km^{-1}), the atmosphere is said to be **conditionally unstable**, meaning it is stable if the air is unsaturated but unstable if air is saturated (if a cloud can form). If the atmosphere is **absolutely stable**, it is stable in both unsaturated and saturated air. Figure 18.2 shows stability criteria for unsaturated and saturated air, and Fig. 18.3 shows how stability is determined in atmospheric layers when each layer has a different ambient environmental temperature profile.

Another method of estimating stability is with **equivalent potential temperature**, which is the potential temperature a parcel of air would have if all its water vapor were condensed and if the latent heat released were used to heat the parcel. It can be found by lifting a parcel from 1000 hPa to low pressure until all water vapor is condensed out, then lowering the parcel dry-adiabatically back to 1000 hPa, as shown in Fig. 18.4. In reality, not all water vapor in a parcel condenses because

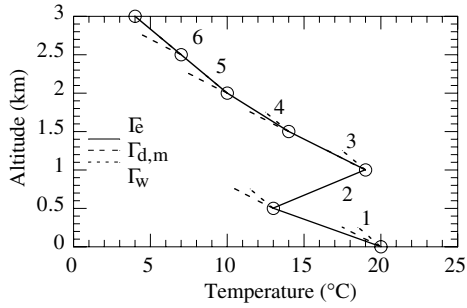

Figure 18.3 Determination of stability in multiple layers of air. Layer 1 is absolutely unstable, layer 2 is absolutely stable and an inversion, layer 3 is dry neutral, layer 4 is conditionally unstable, and layers 5 and 6 are moist neutral. Stability is determined by comparing the slope of the environmental temperature profile (solid line) with the slopes of the dry and pseudoadiabatic lapse-rate profiles.

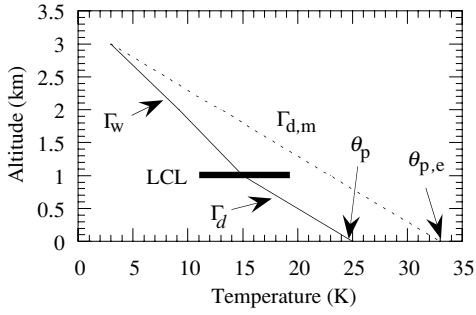

Figure 18.4 Schematic showing the relationship between potential temperature and equivalent potential temperature. Suppose a parcel with $\theta_p = 298.15$ K (25 °C) rises to the LCL dry-adiabatically then to 3 km pseudoadiabatically, at which point it has lost its water vapor. If the parcel descends dry-adiabatically back to the surface, its final potential temperature is $\theta_{p,e} = 306.15$ K (33 °C).

the saturation mass mixing ratio of water always exceeds zero. At high altitudes, though, the additional condensation from an incremental decrease in temperature is negligible, and the pseudoadiabatic lapse rate approaches the dry adiabatic lapse rate.

If the air is initially saturated, as it is above the LCL in Fig. 18.4, the equivalent potential temperature is

$$\theta_{p,e} \approx \theta_p \exp\left(\frac{L_e}{c_{p,d} T} \omega_{v,s}\right) \tag{18.8}$$

where T is the actual initial temperature of the saturated parcel (K), and $\omega_{v,s}$ is the saturation mass mixing ratio of water vapor at that temperature (kg kg^{-1}). If the air is initially unsaturated, as it is below the LCL, equivalent potential temperature is

$$\theta_{p,e} \approx \theta_p \exp\left(\frac{L_e}{c_{p,d} T_{LCL}} \omega_v\right) \tag{18.9}$$

where T_{LCL} is the temperature (K) of the parcel if it were lifted dry-adiabatically to the LCL, and ω_v is the initial, unsaturated mass mixing ratio of water vapor in the parcel.

Stability in unsaturated or saturated air can be found from equivalent potential temperature by defining a variable, $\hat{\theta}_{p,e}$ that equals $\theta_{p,e}$ from (18.8) for either saturated or unsaturated air. For unsaturated air, the temperature in (18.8) is the initial temperature of the environment, not T_{LCL}. In saturated air, the temperature is the saturated-parcel temperature. In both cases, $\omega_{v,s}$ is the saturation mixing ratio at the temperature used. Conceptually, $\hat{\theta}_{p,e}$ is the value of $\theta_{p,e}$ in a hypothetically saturated parcel at the temperature of the parcel. The **stability criteria in terms of** $\hat{\theta}_{p,e}$ are

$$\frac{\partial \hat{\theta}_{p,e}}{\partial z} \begin{cases} < 0 & \text{saturated unstable} \\ = 0 & \text{saturated neutral} \\ > 0 & \text{saturated stable} \end{cases} \tag{18.10}$$

18.3 CLOUD DEVELOPMENT BY FREE CONVECTION

A fog or cloud forms when the air temperature drops below the dew point. Figure 18.5 shows an example of how the environmental, dry-adiabatic, and pseudoadiabatic lapse rates can be applied together with the dew point to estimate the extent of cloud development. If air at the surface is moist but unsaturated, the environment is unstable with respect to dry air. If an external forcing, such as forced convection, occurs, surface air rises. As the parcel rises, the dry-air pressure (p_d) in the parcel decreases because pressure decreases with increasing altitude. If the water-vapor mixing ratio (ω_v) is constant in the parcel, p_v must decrease with increasing height to satisfy $\omega_v = \varepsilon p_v / p_d$. Because p_v decreases, the dew point must also decrease, since it is an increasing function of p_v, as seen from (2.68). The decrease in dew point with increasing altitude is relatively modest (e.g., around 2 K km^{-1}).

The temperature in an unsaturated rising parcel decreases at the dry adiabatic lapse rate. When the dew point and the parcel temperature meet, the air is saturated, condensation occurs, and a cloud forms, as shown in Fig. 18.5. The altitude of cloud formation is the LCL. The temperature at saturation is the **isentropic condensation temperature** (ICT) (K), which usually occurs at the LCL. The ICT is more formally defined as the temperature at which saturation is reached when unsaturated air is cooled adiabatically at a constant mass mixing ratio of water vapor. The ICT can be approximated by substituting T_{IC} and $p_{d,IC}$ for T_D and p_d, respectively, into (2.68),

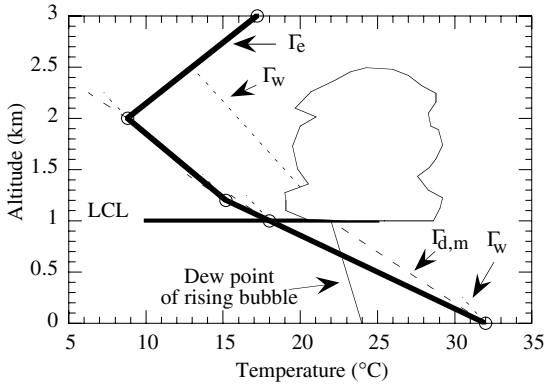

Figure 18.5 Simplified model of cumulus-cloud formation. An unsaturated surface parcel of air at 32 °C in an unstable environment (with environmental lapse rate (Γ_e) is perturbed and starts rising. As it rises, it cools at the dry adiabatic lapse rate ($\Gamma_{d,m}$). The dew point in the parcel decreases at a slower rate. At the lifting condensation level (LCL), the dew point equals the parcel temperature, and a cloud begins to form. Because the parcel temperature is still greater than that of the environment, the parcel continues to rise but cools at the pseudoadiabatic lapse rate (Γ_w). When the parcel temperature equals that of the environment (cloud top), the cloud parcel stops rising.

combining the result with $p_{d,IC} = p_{d,0}\,(T_{IC}/T_0)^{1/\kappa}$ from (2.96), where $p_{d,0}$ is the surface air pressure (not necessarily 1000 hPa) and T_0 is the surface temperature (K), then solving for T_{IC}. The result is

$$T_{IC} \approx \frac{4880.357 - 29.66 \ln\left[\dfrac{\omega_v\, p_{d,0}}{\varepsilon}\left(\dfrac{T_{IC}}{T_0}\right)^{1/\kappa}\right]}{19.48 - \ln\left[\dfrac{\omega_v\, p_{d,0}}{\varepsilon}\left(\dfrac{T_{IC}}{T_0}\right)^{1/\kappa}\right]} \tag{18.11}$$

where ω_v is assumed to be constant between the surface and LCL. The solution must be found iteratively.

Condensation releases latent heat, giving a parcel buoyancy. As a parcel rises above the LCL, as in Fig. 18.5, its temperature and dew point decrease pseudoadiabatically. So long as the temperature of the cloudy air exceeds that of the ambient air, the parcel remains buoyant and continues to rise and expand. When the cloud temperature and ambient temperature equalize, the cloud top decelerates. As shown in Fig. 18.5, the environmental temperature profile, which was unstable below the cloud base and within part of the cloud, must become stable for the cloud top to decelerate.

18.4 ENTRAINMENT

Entrainment is the mixing of relatively cool, dry air from outside a cloud with warm, moist air within the cloud, causing a cloud to evaporate and cool at its edges. Cool air sinks, creating downdrafts at the edges and reducing the height to which the cloud penetrates. Entrainment may also occur at the top or base of a cloud. **Detrainment** is the opposite of entrainment. During detrainment, air leaves the cloud and mixes with air around the cloud, slightly increasing the moisture and heat content of the outside air.

A simple model of the effects of entrainment on a cumulus cloud was developed by Stommel (1947). This model assumes that entrained air continuously enters a rising cloud from its sides and instantaneously mixes uniformly throughout the cloud. In reality, entrainment is not entirely lateral, instantaneous, or continuous (Houze 1993). Stommel's model is a useful tool for one-dimensional studies of clouds and can be used to derive a simplified entrainment term in the thermodynamic energy equation.

The model assumes that entrainment affects cloud temperatures in two ways. First, entrainment forces the cloud to expend energy to heat cool, entrained air to the cloud virtual temperature. The energy (J) used by the cloud for this purpose is

$$\mathrm{d}Q_1^* = -c_{p,\mathrm{d}}(T_\mathrm{v} - \hat{T}_\mathrm{v})\mathrm{d}M_\mathrm{c} \tag{18.12}$$

where T_v is the cloud virtual temperature, $\hat{T}_\mathrm{v}$ is the ambient virtual temperature, and $\mathrm{d}M_\mathrm{c}$ is the mass of ambient dry air plus water vapor entrained in the cloud.

Second, entrainment forces the cloud to expend energy evaporating liquid water to maintain saturation of dry, entrained air. This energy loss (J) is

$$\mathrm{d}Q_2^* = -L_\mathrm{e}(\omega_\mathrm{v,s} - \hat{\omega}_\mathrm{v})\mathrm{d}M_\mathrm{c} \tag{18.13}$$

where $\omega_\mathrm{v,s}$ is the saturation mass mixing ratio of water vapor in the cloud (kg kg^{-1}), and $\hat{\omega}_\mathrm{v}$ is the mass mixing ratio of water vapor outside the cloud.

Third, the entrainment region gains latent heat energy when rising water vapor condenses. The energy gained (J) is

$$\mathrm{d}Q_3^* = -M_\mathrm{c}L_\mathrm{e}\,\mathrm{d}\omega_\mathrm{v,s} \tag{18.14}$$

where M_c is the total mass of air within an entrainment region of the cloud, which consists of dry air, water vapor, and liquid water.

The sum of the three sources and sinks of energy is $\mathrm{d}Q^* = \mathrm{d}Q_1^* + \mathrm{d}Q_2^* + \mathrm{d}Q_3^*$. Substituting (18.12)–(18.14) into this equation gives the total change of energy in the entrainment region of a cloud as

$$\mathrm{d}Q^* = -c_{p,\mathrm{d}}(T_\mathrm{v} - \hat{T}_\mathrm{v})\mathrm{d}M_\mathrm{c} - L_\mathrm{e}(\omega_\mathrm{v,s} - \hat{\omega}_\mathrm{v})\mathrm{d}M_c - M_\mathrm{c}L_\mathrm{e}\,\mathrm{d}\omega_\mathrm{v,s} \tag{18.15}$$

From (2.82) and (2.70), the first law of thermodynamics for this problem requires

$$\mathrm{d}Q^* = M_\mathrm{c}(c_{p,\mathrm{d}}\,\mathrm{d}T_\mathrm{v} - \alpha_\mathrm{a}\,\mathrm{d}p_\mathrm{a}) \tag{18.16}$$

Subtracting (18.16) from (18.15) and rearranging give

$$c_{p,\mathrm{d}}\,\mathrm{d}T_\mathrm{v} - \alpha_\mathrm{a}\,\mathrm{d}p_\mathrm{a} = -[c_{p,\mathrm{d}}(T_\mathrm{v} - \hat{T}_\mathrm{v}) + L_\mathrm{e}(\omega_{\mathrm{v,s}} - \hat{\omega}_\mathrm{v})]\frac{\mathrm{d}M_\mathrm{c}}{M_\mathrm{c}} - L_\mathrm{e}\,\mathrm{d}\omega_{\mathrm{v,s}} \tag{18.17}$$

Dividing (18.17) by $c_{p,\mathrm{d}}T_\mathrm{v}$ and substituting $\alpha_\mathrm{a} = R'T_\mathrm{v}/p_\mathrm{a}$ result in

$$\frac{\mathrm{d}T_\mathrm{v}}{T_\mathrm{v}} - \frac{R'}{c_{p,\mathrm{d}}}\frac{\mathrm{d}p_\mathrm{a}}{p_\mathrm{a}} = -\left[\frac{T_\mathrm{v} - \hat{T}_\mathrm{v}}{T_\mathrm{v}} + \frac{L_\mathrm{e}(\omega_{\mathrm{v,s}} - \omega'_\mathrm{v})}{c_{p,\mathrm{d}}T_\mathrm{v}}\right]\frac{\mathrm{d}M_c}{M_c} - \frac{L_\mathrm{e}\,\mathrm{d}\omega_{\mathrm{v,s}}}{c_{p,\mathrm{d}}T_\mathrm{v}} \tag{18.18}$$

Differentiating (18.18) with respect to height and then substituting $\partial p_\mathrm{a}/\partial z = -\rho_\mathrm{a}g$ and $p_\mathrm{a} = \rho_\mathrm{a}R'T_\mathrm{v}$ give the virtual temperature change with altitude in an entraining cloud as

$$\frac{\partial T_\mathrm{v}}{\partial z} = -\frac{g}{c_{p,\mathrm{d}}} - \left[(T_\mathrm{v} - \hat{T}_\mathrm{v}) + \frac{L_\mathrm{e}}{c_{p,\mathrm{d}}}(\omega_{\mathrm{v,s}} - \hat{\omega}_\mathrm{v})\right]\frac{1}{M_\mathrm{c}}\frac{\partial M_\mathrm{c}}{\partial z} - \frac{L_\mathrm{e}}{c_{p,\mathrm{d}}}\frac{\partial \omega_{\mathrm{v,s}}}{\partial z} \tag{18.19}$$

When no entrainment occurs ($\mathrm{d}M_\mathrm{c} = 0$), (18.19) simplifies to (18.4).

Rearranging (2.103) as

$$\frac{\partial T_\mathrm{v}}{\partial z} = \frac{T_\mathrm{v}}{\theta_\mathrm{v}}\frac{\partial \theta_\mathrm{v}}{\partial z} + \frac{R'T_\mathrm{v}}{c_{p,\mathrm{d}}p_\mathrm{a}}\frac{\partial p_\mathrm{a}}{\partial z} = \frac{T_\mathrm{v}}{\theta_\mathrm{v}}\frac{\partial \theta_\mathrm{v}}{\partial z} - \frac{g}{c_{p,\mathrm{d}}} \tag{18.20}$$

and substituting the result into (18.19) give the change in potential virtual temperature with altitude in an entrainment region of a cloud as

$$\boxed{\frac{\partial \theta_\mathrm{v}}{\partial z} = -\frac{\theta_\mathrm{v}}{T_\mathrm{v}}\left[(T_\mathrm{v} - \hat{T}_\mathrm{v}) + \frac{L_\mathrm{e}}{c_{p,\mathrm{d}}}(\omega_{\mathrm{v,s}} - \hat{\omega}_\mathrm{v})\right]\frac{1}{M_\mathrm{c}}\frac{\partial M_\mathrm{c}}{\partial z} - \frac{\theta_\mathrm{v}}{T_\mathrm{v}}\frac{L_\mathrm{e}}{c_{p,\mathrm{d}}}\frac{\partial \omega_{\mathrm{v,s}}}{\mathrm{d}z}} \tag{18.21}$$

Multiplying through by $\mathrm{d}z$ and dividing through by $\mathrm{d}t$ give the time rate of change of potential virtual temperature in a cloud as

$$\frac{\mathrm{d}\theta_\mathrm{v}}{\mathrm{d}t} = -\frac{\theta_\mathrm{v}}{T_\mathrm{v}}\left[(T_\mathrm{v} - \hat{T}_\mathrm{v}) + \frac{L_\mathrm{e}}{c_{p,\mathrm{d}}}(\omega_{\mathrm{v,s}} - \hat{\omega}_\mathrm{v})\right]\mathrm{E} - \frac{\theta_\mathrm{v}L_\mathrm{e}}{c_{p,\mathrm{d}}T_\mathrm{v}}\frac{\mathrm{d}\omega_{\mathrm{v,s}}}{\mathrm{d}t} \tag{18.22}$$

where $\mathrm{E} = (1/M_\mathrm{c})\,\mathrm{d}M_\mathrm{c}/\mathrm{d}t$ is the **entrainment rate** (s^{-1}) of outside air into the cloud. If a thermal is modeled as a spherical bubble with radius $r_\mathrm{t} \approx 0.2z_\mathrm{c}$ (m), where z_c is the center altitude (m) of the thermal above its starting point, then the rate of entrainment can be approximated with (Houze 1993)

$$\mathrm{E} = \frac{1}{M_\mathrm{c}}\frac{\mathrm{d}M_\mathrm{c}}{\mathrm{d}t} \approx \frac{3}{4\pi r_\mathrm{t}^3}\frac{\mathrm{d}}{\mathrm{d}t}\left(\frac{4\pi r_\mathrm{t}^3}{3}\right) \tag{18.23}$$

Equation (3.76) gave the thermodynamic energy equation with diabatic source and sink terms. One such term is energy release due to condensation, $\mathrm{d}Q_{\mathrm{c/e}} = -L_\mathrm{e}\,\mathrm{d}\omega_{\mathrm{v,s}}$. Two other terms are energy release due to freezing of liquid water and deposition of vapor to ice. These terms can be quantified as $\mathrm{d}Q_{\mathrm{f/m}} = -L_\mathrm{m}\,\mathrm{d}\omega_L$ and $\mathrm{d}Q_{\mathrm{dp/s}} = -L_\mathrm{s}\,\mathrm{d}\omega_{\mathrm{v,I}}$, respectively, where L_m is the latent heat of melting from (2.55), $\mathrm{d}\omega_L$ is the change in mass mixing ratio (kg kg^{-1}) of liquid water upon freezing, L_s

is the latent heat of sublimation from (2.56), $\omega_{v,I} \approx \varepsilon p_{v,I}/p_d$ is the saturation mass mixing ratio of water vapor over an ice surface, which is analogous to (2.67), and $d\omega_{v,I}$ is the change in saturation mass mixing ratio upon sublimation.

Adding these and remaining terms from (3.76) to (18.22) gives the **thermodynamic energy equation in a cloud** as

$$\frac{d\theta_v}{dt} = -\frac{\theta_v}{T_v}\left[(T_v - \hat{T}_v) + \frac{L_e}{c_{p,d}}(\omega_{v,s} - \hat{\omega}_v)\right]E + \frac{1}{\rho_a}(\nabla \cdot \rho_a \mathbf{K}_h \nabla)\,\theta_v + \frac{\theta_v}{c_{p,d}T_v}\left(-L_e\frac{d\omega_{v,s}}{dt} - L_m\frac{d\omega_L}{dt} - L_s\frac{d\omega_{v,I}}{dt} + \frac{dQ_{solar}}{dt} + \frac{dQ_{ir}}{dt}\right) \quad (18.24)$$

Water categories in a cloud include water vapor, liquid water, drizzle, rainwater, cloud ice, snow, graupel, and hail. Conversion from one form of water to another results in a gain or loss of energy, accounted for in the latent-heat terms of (18.24). Bulk parameterizations of the conversion processes are given in Houze (1993), Fowler *et al.* (1996), and Pruppacher and Klett (1997). Size-resolved calculations of these conversion processes are discussed in Section 18.8.

18.5 VERTICAL MOMENTUM EQUATION IN A CLOUD

In a cloud, vertical scalar velocities are affected by local acceleration, gravity, pressure gradients, and turbulence. From (4.75), the vertical momentum equation in Cartesian-altitude coordinates was

$$\frac{dw}{dt} = -g - \frac{1}{\rho_a}\frac{\partial p_a}{\partial z} + \frac{1}{\rho_a}(\nabla \cdot \rho_a \mathbf{K}_m \nabla)\,w \quad (18.25)$$

If $\hat{p}_a$ and $\hat{\rho}_a$ are the pressure and density, respectively, of the air outside a cloud, and if the ambient air is in hydrostatic balance, $\partial \hat{p}_a/\partial z = -\hat{\rho}_a g$. Adding this equation to (18.25) gives

$$\frac{dw}{dt} = -g\frac{\rho_a - \hat{\rho}_a}{\rho_a} - \frac{1}{\rho_a}\frac{\partial(p_a - \hat{p}_a)}{\partial z} + \frac{1}{\rho_a}(\nabla \cdot \rho_a \mathbf{K}_m \nabla)\,w \quad (18.26)$$

where $p_a - \hat{p}_a$ and $\rho_a - \hat{\rho}_a$ are the deviations of cloud pressure and density from ambient pressure and density, respectively.

The **buoyancy factor** is defined as

$$B = -\frac{\rho_a - \hat{\rho}_a}{\rho_a} = -\frac{p_a\hat{T}_v - \hat{p}_a T_v}{p_a\hat{T}_v} = -\frac{\hat{T}_v - T_v}{\hat{T}_v} + \left(\frac{T_v}{\hat{T}_v}\right)\frac{\hat{p}_a - p_a}{p_a} \approx -\frac{\hat{\theta}_v - \theta_v}{\hat{\theta}_v} \quad (18.27)$$

(e.g., Rogers and Yau 1989) where T_v, θ_v, and $\rho_a = p_a/R'T_v$ are the virtual temperature, potential virtual temperature, and density, respectively, of cloudy air, and $\hat{T}_v$, $\hat{\theta}_v$, and $\hat{\rho}_a = \hat{p}_a/R'\hat{T}_v$ are the analogous variables for ambient air. The approximation on the right side of (18.27) was obtained by assuming $(\hat{p}_a - p_a)/p_a$ is small.

If a parcel contains liquid water, as it does above the lifting condensation level, condensate (condensed water) adds a downward force to the parcel. Condensate

in the surrounding air also adds a downward force to the surrounding air. To allow for condensate, the buoyancy factor can be modified to

$$B = -\frac{\rho_a - \hat{\rho}_a}{\rho_a} = -\frac{\hat{\theta}_v(1+\omega_L) - \theta_v(1+\hat{\omega}_L)}{\hat{\theta}_v} \approx \frac{\theta_v - \hat{\theta}_v}{\hat{\theta}_v} - \omega_L \quad (18.28)$$

where ω_L and $\hat{\omega}_L$ are the mass mixing ratios of liquid water in the parcel and ambient air, respectively (kilograms of liquid water per kilogram of dry air). The second expression assumes the liquid-water content of the ambient air is small compared with that in a cloud.

Substituting (18.28) into (18.26) gives the vertical momentum equation as

$$\frac{dw}{dt} = g\left(\frac{\theta_v - \hat{\theta}_v}{\hat{\theta}_v} - \omega_L\right) - \frac{1}{\rho_a}\frac{\partial(p_a - \hat{p}_a)}{\partial z} + \frac{1}{\rho_a}(\nabla \cdot \rho_a \mathbf{K}_m \nabla)w \quad (18.29)$$

From (2.40), (4.48), and (5.38),

$$\frac{1}{\rho_a}\frac{\partial p_a}{\partial z} = -g = -\frac{\partial \Phi}{\partial z} = c_{p,d}\theta_v \frac{\partial P}{\partial z} \quad (18.30)$$

Substituting (18.30) into (18.29) for cloudy and ambient air gives the **vertical momentum equation in a cloud** as

$$\frac{dw}{dt} = g\left(\frac{\theta_v - \hat{\theta}_v}{\hat{\theta}_v} - \omega_L\right) - c_{p,d}\theta_v \frac{\partial(P - \hat{P})}{\partial z} + \frac{1}{\rho_a}(\nabla \cdot \rho_a \mathbf{K}_m \nabla)w \quad (18.31)$$

This equation is similar in several respects to (5.4), the nonhydrostatic vertical momentum equation. As with (5.4), (18.31) can be solved directly, used to derive a diagnostic equation for nonhydrostatic pressure, or solved implicitly.

If the pressure perturbation and the eddy diffusion term are ignored, (18.31) becomes

$$\frac{dw}{dt} = \frac{dw}{dz}\frac{dz}{dt} = \frac{dw}{dz}w = g\left(\frac{\theta_v - \hat{\theta}_v}{\hat{\theta}_v} - \omega_L\right) = gB \quad (18.32)$$

where $w = dz/dt$. Rearranging (18.32) gives $w\,dw = gB\,dz$. Integrating this equation from a reference height z_a, where the vertical scalar velocity is w_a, to height z yields a simplified expression for the vertical scalar velocity in a cloud,

$$w^2 = w_a^2 + 2g\int_{z_a}^{z}\left(\frac{\theta_v - \hat{\theta}_v}{\hat{\theta}_v} - \omega_L\right)dz = w_a^2 + 2g\int_{z_a}^{z} B\,dz \quad (18.33)$$

In this expression, w is determined from the integral of buoyancy between the base of the cloud and the altitude of interest.

18.6 CONVECTIVE AVAILABLE POTENTIAL ENERGY

Equation (18.33) can be modified to give an expression for the **convective available potential energy** (CAPE), which describes the growth potential of a cloud. The CAPE determines the buoyant stability of the atmosphere and correlates positively with growth of and rainfall production in cumulus clouds (Zawadski *et al.* 1981). CAPE ($m^2\ s^{-2}$) is defined as

$$\text{CAPE} = g\int_{z_{\text{LFC}}}^{z_{\text{LNB}}} B\,\mathrm{d}z \approx g\int_{z_{\text{LFC}}}^{z_{\text{LNB}}} \left(\frac{\theta_{\text{v}} - \hat{\theta}_{\text{v}}}{\hat{\theta}_{\text{v}}}\right)\mathrm{d}z \tag{18.34}$$

where z_{LFC} is the **level of free convection** (LFC), z_{LNB} is the **level of neutral buoyancy** (LNB), θ_{v} is the potential virtual temperature of a rising parcel of air, and $\hat{\theta}_{\text{v}}$ is the potential virtual temperature of the environment. The LFC is the altitude at which a parcel of rising air first becomes warmer than the environment. It may be below or above the LCL. The LNB is the altitude near the cloud top at which environmental and cloud temperatures equalize and the cloud is no longer buoyant.

Example 18.2

Estimate CAPE and w for a 10 km-thick cumulonimbus cloud over the ocean and over land if $\theta_{\text{v}} - \hat{\theta}_{\text{v}} \approx 1.5$ K over the ocean, $\theta_{\text{v}} - \hat{\theta}_{\text{v}} \approx 8$ K over land, and the average ambient virtual temperature between 0 and 10 km is $\theta_{\text{v}} = 288$ K in both cases.

SOLUTION

From (18.34), CAPE $\approx 511\ m^2\ s^{-2}$ for the ocean case and $2725\ m^2\ s^{-2}$ for the land case. If ω_{L} is ignored, (18.33) gives $w = 32\ m\ s^{-1}$ for the ocean case and $w = 74\ m\ s^{-1}$ for the land case. These values are higher than observed maximums over the ocean and land, which are 10 and 50 $m\ s^{-1}$, respectively, in thunderstorm clouds.

18.7 CUMULUS PARAMETERIZATIONS

Clouds form over horizontal scales of tens to hundreds of meters. When a model's horizontal resolution is smaller than this, the vertical momentum equation can be used to reproduce cloud structure. The vertical momentum equation can also be used to reproduce much of the structure but not the details of a squall-line convective system for grid resolution of up to 4 km (Weisman *et al.* 1997). Many mesoscale and global models have horizontal resolutions of 4–50 km and 100–600 km, respectively. In both types of models, cloud development is a subgrid-scale phenomenon and must be parameterized.

Several techniques have been developed to estimate the effects of subgrid-scale cumulus clouds on the model-scale environment. These techniques are called **cumulus parameterizations** and require input variables from the model-scale

environment. Important model-scale variables used to predict subgrid effects are horizontal and vertical wind speeds, potential temperatures, and total water mixing ratios. Cumulus parameterizations use these variables to adjust potential temperature, total water, and momentum fields and to predict precipitation rates. The effects of a cumulus parameterization on the model-scale environment are **feedbacks**.

Cumulus parameterizations include moist convective adjustment schemes (e.g., Manabe *et al.* 1965; Miyakoda *et al.* 1969; Krishnamurti and Moxim 1971; Kurihara 1973), Kuo schemes (Kuo 1965, 1974; Anthes 1977; Krishnamurti *et al.* 1980; Molinari 1982), the Arakawa–Schubert scheme (Arakawa and Schubert 1974; Lord and Arakawa 1980; Kao and Ogura 1987; Moorthi and Suarez 1992; Cheng and Arakawa 1997; Ding and Randall 1998), and other schemes (Ooyama 1971; Kreitzberg and Perkey 1976; Fritsch and Chappel 1980; Betts 1986; Betts and Miller 1986; Frank and Cohen 1987; Tiedtke 1989; Kain and Fritsch 1990; Emanuel 1991; Grell 1993; Hack 1994; Kain 2004). Cotton and Anthes (1989) discuss several schemes in detail. Three are briefly described below.

Moist convective adjustment schemes are the most basic cumulus parameterizations. In these schemes, the model-scale vertical temperature profile is adjusted to a critical, stable profile when the relative humidity exceeds a specified value and the temperature profile is unstable with respect to moist air. During adjustment, the temperature profile is adjusted to the pseudoadiabatic rate, the large-scale relative humidity is unchanged, condensed water vapor precipitates, and total moist enthalpy is conserved.

In **Kuo schemes**, rainfall from cumulus convection is assumed to occur following model-scale convergence of moisture. Part of the moisture condenses, releasing latent heat and increasing rainfall. The rest is used to increase the relative humidity of the environment. Cloud dynamics and microphysics are not computed in Kuo schemes, cloud types are not classified, and the altitudes of cloud bases and tops cannot be found.

In the **Arakawa–Schubert scheme** the model-scale environment is divided into a cloud layer, where clouds form, and a subcloud mixed layer. Within the cloud layer, multiple individual clouds are allowed to form. The sum of the individual clouds in a column makes up a cloud ensemble. The cloud ensemble occupies a horizontal area much smaller than the horizontal area of a grid cell. Each cloud in an ensemble has its own fractional entrainment rate, vertical mass flux across the cloud base, and cloud top height. The fractional entrainment rate is defined as the entrainment rate per unit height divided by the vertical mass flux. The ensemble is divided into subensembles, which consist of clouds with similar fractional entrainment rates. Equations are derived for each subensemble and summed over all subensembles to obtain the net effect of the ensemble on the model-scale environment.

Cloud ensembles affect the model-scale environment in two ways. First, when saturated air containing liquid water detrains (escapes) from cloud tops and evaporates, it cools the model-scale environment. Evaporation increases the water-vapor content in the environment. Rates of detrainment differ for different cloud types and cloud-top heights. Second, cumulus convection, which occurs when clouds

grow vertically, induces subsidence between clouds. During subsidence, the model-scale temperature increases and relative humidity decreases.

An advantage of the Arakawa–Schubert scheme is its sophisticated treatment of subgrid-scale clouds. Disadvantages of the original scheme were the omission of convective downdrafts and the assumption that all cloud bases existed in the lowest model layer. Convective downdrafts were added in Cheng and Arakawa (1997). Some versions of the model now permit cloud bases to appear at any altitude (Ding and Randall 1998).

18.8 CLOUD MICROPHYSICS

Prior sections of this chapter described cloud thermodynamics. Here, cloud microphysics, including microphysical interactions of hydrometeor particles with aerosol particles, is discussed. Numerical techniques are given for condensation/deposition of water vapor onto aerosol particles to form liquid and ice cloud particles, coagulation among liquid and ice hydrometeors to form precipitation-sized drops, liquid drop breakup, contact freezing, homogeneous-heterogeneous freezing, evaporation/sublimation of falling drops, evaporative freezing, ice crystal melting, aerosol–hydrometeor coagulation, gas washout, and lightning. Most techniques given here are described in greater detail in Jacobson (2003).

18.8.1 Condensation and ice deposition onto aerosol particles

Liquid cloud drops first form when water vapor condenses onto pre-existing aerosol particles in supersaturated air. Liquid drop formation can occur at temperatures down to −40 °C. Liquid drops that exist below 0 °C are called **supercooled** drops. At subfreezing temperatures, supercooled drop formation competes with ice crystal formation (ice deposition) for the limited amount of water vapor available. In Chapter 16, the equations for condensation and ice deposition of water vapor onto a single aerosol particle and a population of particles were derived. Numerical solutions were given for growth onto one aerosol size distribution. Here, the technique is extended to growth of liquid drops and ice crystals simultaneously onto multiple aerosol size distributions, such as those described by Table 15.1.

The ordinary differential equations for water vapor condensation/evaporation and deposition/sublimation onto multiple aerosol size distributions are

$$\frac{dc_{L,Ni,t}}{dt} = k_{L,Ni,t-h}(C_{v,t} - S'_{L,Ni,t-h}C_{L,s,t-h}) \tag{18.35}$$

$$\frac{dc_{I,Ni,t}}{dt} = k_{I,Ni,t-h}(C_{v,t} - S'_{I,Ni,t-h}C_{I,s,t-h}) \tag{18.36}$$

respectively. The corresponding vapor–hydrometeor mole balance equation is

$$\frac{dC_{v,t}}{dt} = -\sum_{N=1}^{N_T}\sum_{i=1}^{N_B}\left[\begin{array}{l} k_{L,Ni,t-h}(C_{v,t} - S'_{L,Ni,t-h}C_{L,s,t-h}) \\ + k_{I,Ni,t-h}(C_{v,t} - S'_{I,Ni,t-h}C_{I,s,t-h}) \end{array}\right] \tag{18.37}$$

where t and $t - h$ indicate the end and beginning, respectively, of a time step of h seconds, subscripts L and I indicate liquid and ice, respectively, subscripts N

and i indicate the aerosol distribution and size bin in the distribution, respectively, from which the hydrometeor originates, N_T and N_B are the number of aerosol size distributions and the number of size bins in each distribution, respectively, $c_{L,Ni}$ and $c_{I,Ni}$ are mole concentrations (moles per cubic centimeter of air) of liquid water and ice, respectively, in size bin i of aerosol distribution N, C_v is water vapor mole concentration, $C_{L,s}$ and $C_{I,s}$ are saturation vapor mole concentrations over flat, dilute liquid water and ice surfaces, respectively (so are independent of the aerosol distribution and size bin), $S'_{L,Ni}$ and $S'_{I,Ni}$ are the saturation ratios at equilibrium of water vapor over a liquid solution and over an ice surface, respectively, in size bin i of distribution N, and $k_{L,Ni}$ and $k_{I,Ni}$ are the growth rates (s^{-1}) of water vapor to activated **cloud condensation nuclei** (CCN) and **ice deposition nuclei** (IDN), respectively. CCN were defined in Section 16.2.3.3 and IDN were defined in Section 16.8. Briefly, CCN are aerosol particles that can potentially activate into cloud drops if the air is supersaturated with respect to liquid over the particle surface. IDN are aerosol particles that can potentially activate into ice crystals if the air is supersaturated with respect to ice over the particle surface.

Expressions for the **growth rates** are

$$k_{L,Ni} = \frac{n_{lq,Ni} 4\pi r_{Ni} D_v \omega_{v,L,Ni} F_{v,L,Ni}}{\dfrac{m_v D_v \omega_{v,L,Ni} F_{v,L,Ni} L_e S'_{L,Ni} C_{L,s}}{\kappa_a \omega_{h,Ni} F_{h,L,Ni} T} \left(\dfrac{L_e m_v}{R^* T} - 1 \right) + 1} \tag{18.38}$$

$$k_{I,Ni} = \frac{n_{ic,Ni} 4\pi \chi_{Ni} D_v \omega_{v,I,Ni} F_{v,I,Ni}}{\dfrac{m_v D_v \omega_{v,I,Ni} F_{v,I,Ni} L_s S'_{I,Ni} C_{I,s}}{\kappa_a \omega_{h,Ni} F_{h,I,Ni} T} \left(\dfrac{L_s m_v}{R^* T} - 1 \right) + 1} \tag{18.39}$$

which were derived from (16.64) and (16.79), respectively. All terms are evaluated at time $t - h$. In these equations, $n_{lq,Ni}$ and $n_{ic,Ni}$ are the number concentrations (particles cm^{-3}) of CCN and IDN, respectively, in each size bin of each aerosol distribution.

Other terms in (18.38) and (18.39) include the following: m_v is the molecular weight of water vapor (g mol^{-1}), D_v is the diffusion coefficient of water vapor in air (cm^2 s^{-1}) (from (16.17) with subscript v substituted for subscript q to indicate water vapor), γ_{Ni} is particle radius (cm), χ_{Ni} is the ice crystal electrical capacitance (cm) (from (16.77)), ω_v and ω_h are dimensionless factors for water vapor and energy, respectively, that account for corrections for collision geometry and sticking probability during growth (from (16.19) and (16.27), respectively), F_v is the dimensionless ventilation coefficient for vapor (from (16.24) for liquid and (16.78) for ice), F_h is the dimensionless ventilation coefficient for energy (from (16.31) for liquid and (16.78) for ice), L_e and L_s are latent heats of evaporation and sublimation, respectively (J g^{-1}), κ_a is the thermal conductivity of moist air (J cm^{-1} s^{-1} K^{-1}), T is temperature (K), and R^* is the universal gas constant (8.31451 J mol^{-1} K^{-1}).

The size bins included in (18.36) and (18.37) depend not only on whether CCN or IDN are present but also on whether conditions for activation of particles in a given size bin are met. CCN/IDN activation is determined by solving a Köhler

equation similar to (16.40) but assuming (a) the Kelvin and solute effects affect the saturation ratio at equilibrium over liquid water, (b) multiple solutes dissolved in solution affect the saturation ratio over liquid water, and (c) only the Kelvin effect affects the saturation ratio at equilibrium over ice. The **Köhler equations** under such conditions are

$$S'_{\mathrm{L},Ni,t-h} \approx 1 + \frac{2\sigma_{\mathrm{L},Ni,t-h} m_\mathrm{v}}{r_{Ni} R^* T \rho_\mathrm{L}} - \frac{3 m_\mathrm{v}}{4\pi r_{Ni}^3 \rho_\mathrm{L} n_{Ni,t-h}} \sum_{q=1}^{N_\mathrm{s}} c_{q,Ni,t-h} \tag{18.40}$$

$$S'_{\mathrm{I},Ni,t-h} \approx 1 + \frac{2\sigma_{\mathrm{I},Ni,t-h} m_\mathrm{v}}{r_{Ni} R^* T \rho_\mathrm{I}} \tag{18.41}$$

where $\sigma_{\mathrm{L},Ni}$ and $\sigma_{\mathrm{I},Ni}$ are the surface tensions over liquid and ice, respectively (dyn $\mathrm{cm}^{-1} = \mathrm{g\ s}^{-2}$), m_v is the molecular weight of water (g mol^{-1}), ρ_L and ρ_I are the densities of liquid water and ice, respectively (g cm^{-3}), r_{Ni} is particle radius (cm), R^* is the universal gas constant ($8.314\,51 \times 10^7$ g cm^2 s^{-2} mol^{-1} K^{-1}), T is temperature (K), n_{Ni} is the total number concentration of aerosol particles of size i in distribution N (particles cm^{-3}-air), N_s is the number of soluble components in an aerosol particle, and $c_{q,Ni}$ is the mole concentration of soluble component q in aerosol particles of size i in distribution N. Soluble components include dissociated or undissociated electrolytes and undissociated soluble molecules. The surface tension itself depends on solute concentration, as discussed in Section 16.2.3.1.

Equation (18.40) can be rewritten as

$$S'_{\mathrm{L},Ni,t-h} \approx 1 + \frac{a_{\mathrm{L},Ni,t-h}}{r_{Ni}} - \frac{b_{\mathrm{L},Ni,t-h}}{r_{Ni}^3} \tag{18.42}$$

where

$$a_{\mathrm{L},Ni,t-h} = \frac{2\sigma_{\mathrm{L},Ni,t-h} m_\mathrm{v}}{R^* T \rho_\mathrm{L}} \qquad b_{\mathrm{L},Ni,t-h} = \frac{3 m_\mathrm{v}}{4\pi \rho_\mathrm{L} n_{Ni,t-h}} \sum_{q=1}^{N_\mathrm{s}} c_{q,Ni,t-h} \tag{18.43}$$

Taking the partial derivative of (18.42) with respect to radius and setting it to zero, solving for the radius, and substituting the result back into (18.42) give the **critical radius for growth** (cm) and **critical saturation ratio** for liquid cloud drop activation as

$$r^*_{\mathrm{L},Ni,t-h} = \sqrt{\frac{3 b_{\mathrm{L},Ni,t-h}}{a_{\mathrm{L},Ni,t-h}}} \qquad S^*_{\mathrm{L},Ni,t-h} = 1 + \sqrt{\frac{4 a^3_{\mathrm{L},Ni,t-h}}{27 b_{\mathrm{L},Ni,t-h}}} \tag{18.44}$$

respectively. A CCN activates into a liquid cloud drop under the following conditions:

$$\text{CCN activation} \begin{cases} r_{Ni} > r^*_{\mathrm{L},Ni} & \text{and} \quad C_{\mathrm{v},t-h} > S'_{\mathrm{L},Ni,t-h} C_{\mathrm{L,s},t-h} \\ & \text{or} \\ r_{Ni} \le r^*_{\mathrm{L},Ni} & \text{and} \quad C_{\mathrm{v},t-h} > S^*_{\mathrm{L},Ni,t-h} C_{\mathrm{L,s},t-h} \end{cases} \tag{18.45}$$

An IDN activates when

$$\text{IDN activation} \quad C_{v,t-h} > S'_{I,Ni,t-h} C_{I,s,t-h} \tag{18.46}$$

Above 0 °C, no ice can form and only (18.45) applies. Between −40 and 0 °C, condensation competes with ice deposition, but the saturation vapor mole concentration over ice is less than that over liquid ($C_{I,s} < C_{L,s}$), so ice growth is favored. Below −40 °C, no liquid drops can form, and only (18.46) applies.

Example 18.3

Calculate the critical radius and critical supersaturation when a population of 100 aerosol particles cm^{-3}, all with initial radius of 0.3 μm, contains 2×10^{-16} mol cm^{-3}-air of an organic compound that does not dissociate. Assume $T = 298.15$ K.

SOLUTION

The initial molality of the organic compound in solution is

$$\mathbf{m} = \frac{c}{n\upsilon\rho_w} = \frac{2 \times 10^{-16} \dfrac{\text{mol}}{\text{cm}^3} \times 1000 \dfrac{\text{g}}{\text{kg}}}{100 \dfrac{\text{partic.}}{\text{cm}^3} \times \dfrac{4}{3}\pi \left(3 \times 10^{-5}\,\text{cm}\right)^3 \times 1 \dfrac{\text{g}}{\text{cm}^3}} = 0.0177 \dfrac{\text{mol}}{\text{kg}}$$

From (14.19), the surface tension of liquid water at 298.15 K is 72.225 dyn cm^{-1}. From (16.34), the surface tension of water containing 0.0177 mol kg^{-1} of an organic compound is 58.31 dyn cm^{-1}. From (18.43),

$$a_L = \frac{2\sigma_L m_v}{R^* T \rho_L} = \frac{2 \times 58.31 \dfrac{\text{dyn}}{\text{cm}} \times 18.02 \dfrac{\text{g}}{\text{mol}}}{8.31451 \times 10^7 \dfrac{\text{g cm}^2}{\text{s}^2\,\text{mol K}} \times 298.15\,\text{K} \times 1 \dfrac{\text{g}}{\text{cm}^3}} 1 \frac{\text{g cm}}{\text{dyn s}^2}$$

$$= 8.478 \times 10^{-8}\,\text{cm}$$

$$b_L = \frac{3 m_w c}{4\pi \rho_L n} = \frac{3 \times 18.02 \dfrac{\text{g}}{\text{mol}} \times 2 \times 10^{-16} \dfrac{\text{mol}}{\text{cm}^3}}{4\pi \times 1 \dfrac{\text{g}}{\text{cm}^3} \times 100 \dfrac{\text{partic.}}{\text{cm}^3}} = 8.604 \times 10^{-18}\,\text{cm}^3$$

respectively. Finally, from (18.44), the critical radius and critical saturation ratio are

$$r_L^* = \sqrt{\frac{3b_L}{a_L}} = 1.744 \times 10^{-5}\,\text{cm} = 0.174\,\mu\text{m}$$

$$S_L^* = 1 + \sqrt{\frac{4a_L^3}{27b_L}} = 1.0032$$

respectively. Since the radius of the population of aerosol particles exceeds the critical radius, the population will activate for any saturation ratio greater than that over an individual particle surface.

A noniterative numerical solution to (18.35)–(18.37) is obtained by integrating (18.35) and (18.36) for one size bin over a time step h, yielding

$$c_{\mathrm{L},Ni,t} = c_{\mathrm{L},Ni,t-h} + hk_{\mathrm{L},Ni,t-h}(C_{\mathrm{v},t} - S'_{\mathrm{L},Ni,t-h}C_{\mathrm{L,s},t-h}) \tag{18.47}$$

$$c_{\mathrm{I},Ni,t} = c_{\mathrm{I},Ni,t-h} + hk_{\mathrm{I},Ni,t-h}(C_{\mathrm{v},t} - S'_{\mathrm{I},Ni,t-h}C_{\mathrm{I,s},t-h}) \tag{18.48}$$

respectively, where the final gas mole concentration in both cases, $C_{\mathrm{v},t}$, is currently unknown. Final hydrometeor and gas concentrations are constrained by the gas–hydrometeor mole-balance equation,

$$C_{\mathrm{v},t} + \sum_{N=1}^{N_\mathrm{T}}\sum_{i=1}^{N_\mathrm{B}}(c_{\mathrm{L},Ni,t} + c_{\mathrm{I},Ni,t}) = C_{\mathrm{v},t-h} + \sum_{N=1}^{N_\mathrm{T}}\sum_{i=1}^{N_\mathrm{B}}(c_{\mathrm{L},Ni,t-h} + c_{\mathrm{I},Ni,t-h}) = C_{\mathrm{tot}} \tag{18.49}$$

Substituting (18.47) and (18.48) into (18.49) and solving for $C_{\mathrm{v},t}$ give a generalized solution for simultaneous condensation/evaporation and deposition/sublimation,

$$C_{\mathrm{v},t} = \frac{C_{\mathrm{v},t-h} + h\sum_{N=1}^{N_\mathrm{T}}\sum_{i=1}^{N_\mathrm{B}}(k_{\mathrm{L},Ni,t-h}S'_{\mathrm{L},Ni,t-h}C_{\mathrm{L},s,t-h} + k_{\mathrm{I},Ni,t-h}S'_{\mathrm{I},Ni,t-h}C_{\mathrm{I,s},t-h})}{1 + h\sum_{N=1}^{N_\mathrm{T}}\sum_{i=1}^{N_\mathrm{B}}(k_{\mathrm{L},Ni,t-h} + k_{\mathrm{I},Ni,t-h})} \tag{18.50}$$

Since $C_{\mathrm{v},t}$ from (18.50) can exceed the maximum gas concentration in the system, C_{tot}, $C_{\mathrm{v},t}$ must be set to the smaller of itself and C_{tot}. Equation (18.50) does not allow $C_{\mathrm{v},t}$ to fall below zero in any situation. Once $C_{\mathrm{v},t}$ is solved, it is substituted back into (18.47) and (18.48) to give the final hydrometeor concentration in each size bin of each distribution. Since (18.47) and (18.48) can result in negative concentrations or concentrations above the maximum, two limits are placed sequentially after both equations are solved among all size bins. The first is

$$c_{\mathrm{L},Ni,t} = \mathrm{MAX}\,(c_{\mathrm{L},Ni,t}, 0) \qquad c_{\mathrm{I},Ni,t} = \mathrm{MAX}\,(c_{\mathrm{I},Ni,t}, 0) \tag{18.51}$$

which is solved for all size bins. The second, shown for liquid (the equation for ice uses $c_{\mathrm{I},Ni,t} - c_{\mathrm{I},Ni,t-h}$ instead of $c_{\mathrm{L},Ni,t} - c_{\mathrm{L},Ni,t-h}$ in the rightmost term) is

$$c_{\mathrm{L},Ni,t} = \frac{\left\{C_{\mathrm{v},t-h} - C_{\mathrm{v},t} + \sum_{N=1}^{N_\mathrm{T}}\sum_{i=1}^{N_\mathrm{B}}\left\{\begin{array}{l}\mathrm{MAX}\,[c_{\mathrm{L},Ni,t-h} - c_{\mathrm{L},Ni,t}, 0]\\ +\mathrm{MAX}\,[c_{\mathrm{I},Ni,t-h} - c_{\mathrm{I},Ni,t}, 0]\end{array}\right\}\right\}}{\sum_{N=1}^{N_\mathrm{T}}\sum_{i=1}^{N_\mathrm{B}}\left\{\begin{array}{l}\mathrm{MAX}\,[c_{\mathrm{L},Ni,t} - c_{\mathrm{L},Ni,t-h}, 0]\\ +\mathrm{MAX}\,[c_{\mathrm{I},Ni,t} - c_{\mathrm{I},Ni,t-h}, 0]\end{array}\right\}} \times (c_{\mathrm{L},Ni,t} - c_{\mathrm{L},Ni,t-h}) \tag{18.52}$$

where all $c_{\mathrm{L},N,i,t}$ and $c_{\mathrm{I},N,i,t}$ values on the right side of the equation are determined from (18.51) after it has been solved for all size bins. The solution in (18.47)–(18.52) is exactly mole conserving between water vapor and all liquid and ice

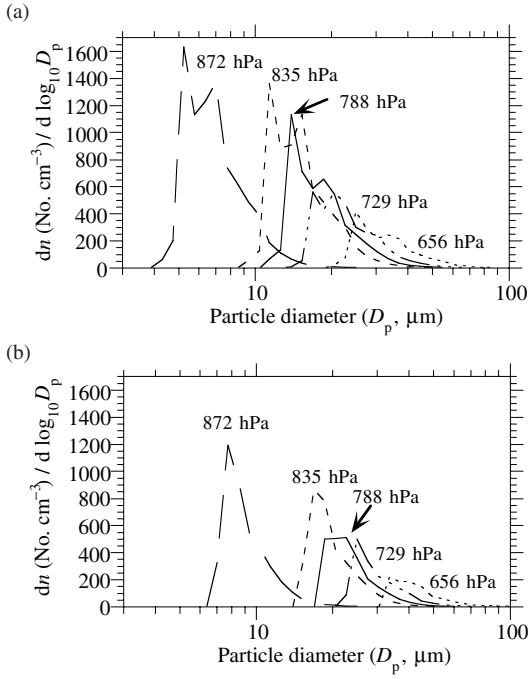

Figure 18.6 Condensed water onto 16 CCN distributions simultaneously in each of five layers in which the temperature was above 0 °C during a one-dimensional simulation when cloud activation was (a) determined from Equation (18.45) and (b) assumed to occur for all particles >0.2 μm in diameter regardless of their composition. From Jacobson (2003).

hydrometeors in all size bins of all distributions under all conditions and is noniterative.

Figure 18.6(a) shows a calculation of cloud drop growth at five altitudes. At each altitude, water vapor condensed onto the 16 aerosol distributions similar to those shown in Table 15.1, where CCN activation in each distribution was determined from (18.45). Liquid drop concentrations were summed over the 16 distributions in each layer to generate the figure. Figure 18.6(b) shows a similar calculation, but when all particles >0.2 μm in diameter were allowed to activate, regardless of their compositions. A comparison of the figures suggests that treatment of multiple distributions, each with different activation characteristics, produced dual peaks in the resulting cloud drop size distribution. Such dual peaks, which have also been observed (e.g., Pruppacher and Klett 1997, Figs. 2.25 and 2.12(a)), arose because different distributions activate at different diameters, causing discontinuities in the summed size distribution. When the activation diameter was held constant over all distributions (Fig. 18.6(b)), only one peak arose for each layer. Single peaks are also widely observed, suggesting that whether one or two peaks exist may depend

on the activation properties of the underlying aerosol particles, which depend on composition, surface tension, and density.

18.8.2 Hydrometeor–hydrometeor coagulation

In Chapter 15, the integrodifferential coagulation equation and a numerical solution to it were given. Here, the solution is extended to liquid and ice hydrometeor distributions. Hydrometeor–hydrometeor coagulation (also called collision-coalescence) is the main process producing precipitation in warm clouds.

The scheme described here is semiimplicit, volume conserving, volume-concentration conserving, positive-definite, unconditionally stable, and noniterative, with no limitation on time step. Other schemes that have been used to solve coagulation in clouds include those of Tzivion *et al.* (1987), Hounslow *et al.* (1988), Lister *et al.* (1995), and Bott (2000). All such schemes conserve various properties, but are explicit; thus, their time step is limited by stability constraints.

The interactions considered here include liquid–liquid, ice–ice, and graupel–graupel self coagulation, liquid–ice, liquid–graupel, and ice–graupel heterocoagulation, and coagulation of aerosol components contained within the hydrometeor distributions. Whereas the initial sources of liquid and ice hydrometeors in the atmosphere are condensation and ice deposition, respectively, the initial source of graupel is ice–liquid coagulation. The solution method here accounts for all coagulation interactions simultaneously; thus ice–liquid heterocoagulation for example, is solved together with liquid–liquid self-coagulation.

The final volume concentration of component x, in particles of hydrometeor distribution Y in bin k at time t due to coagulation is determined with

$$v_{x,Yk,t} = \frac{v_{x,Yk,t-h} + h\,(T_{x,Yk,t,1} + T_{x,Yk,t,2})}{1 + hT_{x,Yk,t,3}} \tag{18.53}$$

$$T_{x,Yk,t,1} = \sum_{M=1}^{N_H} \left[P_{Y,M} \sum_{j=1}^{k} \left(n_{Mj,t-h} \sum_{i=1}^{k-1} f_{Yi,Mj,Yk} \beta_{Yi,Mj,t-h} v_{x,Yi,t} \right) \right]$$

$$T_{x,Yk,t,2} = \sum_{M=1}^{N_H} \sum_{I=1}^{N_H} \left[Q_{I,M,Y} \sum_{j=1}^{k} \left(n_{Mj,t-h} \sum_{i=1}^{k} f_{Ii,Mj,Yk} \beta_{Ii,Mj,t-h} v_{x,Ii,t} \right) \right]$$

$$T_{x,Yk,t,3} = \sum_{j=1}^{N_C} \left[\sum_{M=1}^{N_H} [(1 - L_{Y,M})(1 - f_{Yk,Mj,Yk}) + L_{Y,M}] \beta_{Yk,Mj,t-h} n_{Mj,t-h} \right]$$

where N_H is the total number of hydrometeor distributions and N_C is the number of size bins in each hydrometeor distribution. In this case, $N_H = 3$, where distributions $Y = \text{lq} = 1$ for liquid, $Y = \text{ic} = 2$ for ice, and $Y = \text{gr} = 3$ for graupel. The equation applies when v_x is either the total hydrometeor volume concentration ($v_{T,lq}$, $v_{T,ic}$, or $v_{T,gr}$), the volume concentration of liquid water or ice in a hydrometeor

Table 18.3 Values of $P_{Y,M}$ and $L_{Y,M}$ when coagulation is treated among liquid (lq), ice (ic), and graupel (gr) size distributions.

	M		
Y	**lq**	**ic**	**gr**
$P_{Y,M}$			
lq	1	0	0
ic	0	1	0
gr	1	1	1
$L_{Y,M}$			
lq	0	1	1
ic	1	0	1
gr	0	0	0

($\upsilon_{\mathrm{L,lq}}$, $\upsilon_{\mathrm{I,ic}}$, or $\upsilon_{\mathrm{I,gr}}$), the volume concentration of an aerosol solution incorporated within a hydrometeor ($\upsilon_{\mathrm{s,lq}}$, $\upsilon_{\mathrm{s,ic}}$, or $\upsilon_{\mathrm{s,gr}}$), or the volume concentration of any individual aerosol component incorporated within a hydrometeor ($\upsilon_{q,\mathrm{lq}}$, $\upsilon_{q,\mathrm{ic}}$, or $\upsilon_{q,\mathrm{gr}}$). If it is total volume concentration, then total hydrometeor number concentration (n_{lq}, n_{ic}, or n_{gr}) equals total hydrometeor volume concentration divided by the single-particle volume in the bin. For example,

$$n_{\mathrm{lq},k,t} = \frac{\upsilon_{\mathrm{T,lq},k,t}}{\upsilon_{\mathrm{lq},k}} \tag{18.54}$$

Alternatively, both sides of (18.53) can be divided by single-particle volume to solve for number concentration directly, and the result is identical.

In (18.53), $f_{Ii,Mj,Yk}$ is the volume fraction of the summed volume of two single particles, $V_{Ii,Mj} = \upsilon_{Ii} + \upsilon_{Mj}$, from distributions I and M, partitioned to a fixed size bin k of distribution Y. Each $V_{Ii,Mj}$ is fractionated between two fixed bins in a volume- and number-conserving manner. The volume fractions are

$$f_{Ii,Mj,Yk} = \begin{cases} \left(\dfrac{\upsilon_{Yk+1} - V_{Ii,Mj}}{\upsilon_{Yk+1} - \upsilon_{Yk}}\right)\dfrac{\upsilon_{Nk}}{V_{Ii,Mj}} & \upsilon_{Yk} \le V_{Ii,Mj} < \upsilon_{Yk+1} \quad k < N_{\mathrm{C}} \\ 1 - f_{Ii,Mj,Yk-1} & \upsilon_{Yk-1} < V_{Ii,Mj} < \upsilon_{Yk} \quad k > 1 \\ 1 & V_{Ii,Mj} \ge \upsilon_{Yk} \quad k = N_{\mathrm{C}} \\ 0 & \text{all other cases} \end{cases} \tag{18.55}$$

Finally, P, Q, and L are either 1 or 0, depending on the coagulation interactions accounted for. The parameter $P_{Y,M} = 1$ if particles in distribution Y coagulating with particles in distribution M produce larger particles in distribution Y. The upper part of Table 18.3 lists the values of $P_{Y,M}$ when liquid, ice, and graupel distributions are considered. The parameter $Q_{I,M,Y} = 1$ if particles in distribution I coagulating with particles in distribution M produce particles in distribution Y, and $I \neq M$ and $I \neq Y$. For example, $Q_{\mathrm{lq,ic,gr}}$, $Q_{\mathrm{lq,gr,gr}}$, $Q_{\mathrm{ic,lq,gr}}$, and $Q_{\mathrm{ic,gr,gr}} = 1$, but all other interactions are zero. The parameter $L_{Y,M} = 1$ if particles in distribution Y

coagulating with particles in distribution M do not produce particles in distribution Y. The lower part of Table 18.3 lists the values of $L_{Y,M}$.

In (18.53), term T_1 accounts for production of larger liquid, ice, and graupel particles from self-coagulation and production of larger graupel from liquid and ice heterocoagulation with graupel. Term T_2 accounts for production of graupel from liquid heterocoagulation with ice. The first part of term T_3 accounts for self-coagulation loss of liquid, ice, and graupel to form larger sizes. The second part of the same term accounts for loss of liquid and ice by heterocoagulation with graupel to form more graupel.

Equation (18.53) is solved in a special order. Distributions that have no coagulation production from other distributions (e.g., the liquid and ice distributions) are solved first, followed by distributions with production terms from previously solved distributions (e.g., the graupel distribution). Within each distribution, equations are solved from bin $k = 1 \ldots N_C$. The volume concentrations of individual components within a distribution can be solved in any order. To minimize computer time, all calculations involving a zero value of f, P, Q, or L are eliminated ahead of time.

The total hydrometeor–hydrometeor coagulation kernel (cm^3 particle^{-1} s^{-1}) is

$$\beta_{Ii,Jj} = E_{\text{coal},Ii,Jj} K_{Ii,Jj} \tag{18.56}$$

where $E_{\text{coal},Ii,Jj}$ is a coalescence efficiency (dimensionless) and $K_{Ii,Jj}$ is a collision kernel (cm^3 particle^{-1} s^{-1}) accounting for several physical processes causing collision in the atmosphere. Collision kernels are given in Section 15.6 for Brownian motion, convective Brownian motion enhancement, gravitational collection, turbulent inertial motion, turbulent shear, van der Waals/viscous forces, particle shape, thermophoresis, diffusiophoresis, and electric charge. Coalescence efficiencies are discussed in Section 15.6.8.

18.8.3 Drop breakup

When liquid raindrops grow sufficiently large by coagulation, they become unstable and break up, either spontaneously or upon collision with other hydrometeor particles. One method of solving for drop breakup is to add breakup terms to the coagulation solution (e.g., List and Gillespie 1976). This method requires a fragment probability distribution for the interaction of each hydrometeor pair. A second method is simply to assume drops break up once they reach a critical size (e.g., Danielsen *et al.* 1972). This method requires a breakup distribution, which is similar to a fragment probability distribution, except that a breakup distribution does not consider the physics behind breakup. In addition, it assumes all drops break up once they reach a certain size whereas, in reality, some do not breakup until they are larger. On the other hand, fragment probabilities contain uncertainties as well.

Table 18.4 Polynomial coefficients for drop breakup for use in (18.57)

	$300 < D \leq 1290$ μm	$1290 < D \leq 5160$ μm
A_0	0.53098621799986	6.5418838298481
A_1	−0.0036655403240035	−0.0043878127949574
A_2	0.0000077765141976619	0.0000010066406670884
A_3	$-2.9695029431377 \times 10^{-9}$	$-7.771123366063 \times 10^{-11}$

Source: Jacobson (2003).

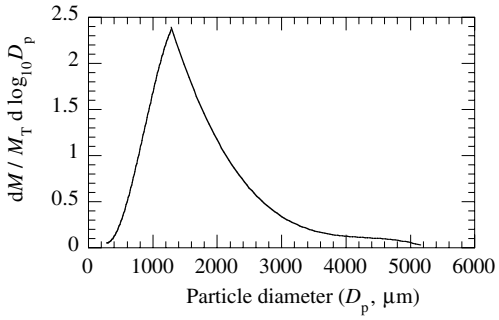

Figure 18.7 Large-drop breakup distribution from (18.57).

Figure 18.7 shows a raindrop breakup distribution obtained by curve-fitting a measured breakup distribution from Danielsen *et al.* (1972). The polynomial fit used to produce the figure is

$$\frac{\mathrm{d}M}{M_\mathrm{T}\,\mathrm{d}\log_{10} D} = A_0 + D[A_1 + D(A_2 + DA_3)] \tag{18.57}$$

where dM is incremental liquid water mass in a size increment, M_T is liquid water mass summed over all sizes, D is particle diameter (μm), and Table 18.4 gives the coefficients used in the equation.

In a model, drop breakup may be assumed to occur when drops exceed 5-mm in diameter. Upon breakup, mass fractions of the breakup drop are assigned to each of several hydrometeor size bins. In such a case, the mass fraction of each breakup drop going to model size bin k of diameter $D = d_k$ is

$$f_{M,k} = \frac{\dfrac{\mathrm{d}M}{M_\mathrm{T}\,\mathrm{d}\log_{10} d_k}\mathrm{d}\log_{10} d_k}{\displaystyle\sum_{k=1}^{N_\mathrm{C}}\left(\frac{\mathrm{d}M}{M_T\,\mathrm{d}\log_{10} d_k}\mathrm{d}\log_{10} d_k\right)} = \frac{[A_0 + d_k(A_1 + d_k(A_2 + d_k A_3))]\mathrm{d}\log_{10} d_k}{\displaystyle\sum_{k=1}^{N_\mathrm{C}}([A_0 + d_k(A_1 + d_k(A_2 + d_k A_3))]\mathrm{d}\log_{10} d_k)} \tag{18.58}$$

Finally, the number concentration of drops added to each bin of diameter-width $\mathrm{d}\log_{10} d_k$ due to the breakup of a single drop of diameter $d_\mathrm{orig} > 5$mm is $\Delta n_k = f_{M,k}(d_\mathrm{orig}/d_k)^3$.

18.8.4 Contact freezing

Contact freezing is a mechanism by which an aerosol ice contact nucleus (ICN) collides with the surface of a liquid drop at a subfreezing temperature and causes the drop to freeze spontaneously. This process can be treated numerically by coagulating size-resolved ICN with size-resolved liquid hydrometeors. As applied here, the calculation assumes that if an ICN collides with a liquid drop, the drop and its aerosol inclusions are transferred to the graupel distribution.

The loss of liquid hydrometeor total volume concentration ($x = T$) and aerosol component volume concentration ($x = q$) due to contact freezing is

$$v_{x,\mathrm{lq},k,t} = \frac{v_{x,\mathrm{lq},k,t-h}}{1 + hT_{x,k,t,3}} \tag{18.59}$$

and the corresponding gain of graupel is

$$v_{x,\mathrm{gr},k,t} = v_{x,\mathrm{gr},k,t-h} + v_{x,\mathrm{lq},k,t} hT_{x,k,t,3} \tag{18.60}$$

In these equations, the implicit loss coefficient (s^{-1}) of drops due to their heterocoagulation with ICN is

$$T_{x,k,t,3} = F_T \sum_{j=1}^{N_\mathrm{C}} \left[\sum_{N=1}^{N_\mathrm{T}} \beta_{Yk,Nj,t-h} F_{\mathrm{ICN},Nj} n_{Nj,t-h} \right] \tag{18.61}$$

where $F_{\mathrm{ICN},Nj}$ is the ratio of the number concentration of contact nuclei to that of total particles in an aerosol size bin, F_T is a temperature-dependent parameter that reduces the rate of contact nucleation at high temperatures, and $\beta_{Yk,Nj,t-h}$ is the kernel (cm^3 $\mathrm{particle}^{-1}$ s^{-1}) for coagulation between liquid drops and aerosol particles (Section 15.6). Equations (18.59) and (18.60) are solved in the order $k = 1 \ldots N_\mathrm{C}$, where N_C is the number of hydrometeor size bins per hydrometeor distribution. The **final number concentrations** of liquid and graupel hydrometeors in each bin of each distribution are

$$n_{\mathrm{lq},k,t} = \frac{v_{T,\mathrm{lq},k,t}}{v_{\mathrm{lq},k}} \tag{18.62}$$

$$n_{\mathrm{gr},k,t} = \frac{v_{T,\mathrm{gr},k,t}}{v_{\mathrm{gr},k}} \tag{18.63}$$

respectively. **The temperature-dependence parameter** in (18.61) is a fraction,

$$F_T = \begin{cases} 0 & T > -3\,^\circ\mathrm{C} \\ -(T+3)/15 & -18 < T < -3\,^\circ\mathrm{C} \\ 1 & T < -18\,^\circ\mathrm{C} \end{cases} \tag{18.64}$$

where T is in °C. This equation was obtained by noting that Fig. 2 of Pitter and Pruppacher (1973) shows that kaolinite and montmorillonite contact freeze 100 percent of drops at −18 °C and 0 percent of drops at −3 °C. The product, $F_T F_{\mathrm{ICN},Nj} n_{Nj,t-h}$, is the number concentration of ICN in a given size bin of a given aerosol size distribution at a given temperature. The fractional number of ICN ($F_{\mathrm{ICN},Nj}$) should be larger than the fractional number of IDN in each size bin of a

distribution since only few aerosol types can serve as IDN but many can serve as ICN.

Contact freezing freezes a higher proportion of small drops than large drops. Although the coagulation rate coefficient of an aerosol particle with a liquid drop generally increases with increasing size, the number concentration of large drops decreases at a greater rate than the coagulation rate coefficient increases with increasing size, causing the aerosol–liquid drop coagulation rate (rate coefficient multiplied by number concentrations of colliding particles) to decrease with increasing size.

Even though contact freezing freezes primarily small drops, the number concentration of aerosol particles in the upper troposphere is sufficiently small that contact freezing has relatively little effect on the size distribution of liquid or graupel in the upper troposphere. In cold, lower-tropospheric regions in which aerosol particle concentrations are high, though (e.g., in populated northern latitude regions during winter), contact freezing is a more important freezing mechanism than in the upper troposphere.

Example 18.4

Calculate the fraction of the number concentration of 40-μm-radius liquid drops that contact freeze during one hour in the presence of 10^3 aerosol particles cm^{-3}. Assume the temperature is $-20\,^{\circ}C$, the coagulation rate coefficient is 10^{-4} cm^3 $particle^{-1}$ s^{-1}, and a maximum of 5 percent of the aerosol particles present can serve as contact nuclei.

SOLUTION

The fractional number concentration of liquid drops that freeze is

$$1 - \frac{n_{\mathrm{lq},t}}{n_{\mathrm{lq},t-h}} = 1 - \frac{v_{T,\mathrm{lq},t}}{v_{T,\mathrm{lq},t-h}} = 1 - \frac{1}{1 + hF_T F_{\mathrm{ICN}}\beta}$$

$$= 1 - \frac{1}{1 + 3600\mathrm{s} \times 1 \times 0.05 \times 10^{-4}\,\dfrac{\mathrm{cm}^3}{\mathrm{partic.\ s}} \times 10^3\,\dfrac{\mathrm{partic.}}{\mathrm{cm}^3}} = 0.947$$

Thus, nearly 95 percent of liquid drops contact freeze within an hour under the conditions specified.

18.8.5 Homogeneous and heterogeneous freezing

Two other methods of freezing liquid drops are homogeneous and heterogeneous freezing. **Heterogeneous freezing** is triggered when an aerosol particle, called an **ice immersion nucleus** (IIN) in this case, enters a liquid drop. Once immersed in the drop, the IIN's surface serves as a site for liquid water heterogeneous nucleation to ice. Once an ice cluster forms on the IIN surface, it grows rapidly, engulfing the IIN and eventually converting all the liquid water in the drop to ice. Often, multiple IIN

act simultaneously, enhancing the freezing rate of the drop. **Homogeneous freezing** is caused by the homogeneous nucleation of ice crystals within or on the surface of a liquid drop in the absence of an IIN. Once a homogeneously nucleated cluster forms, it grows until the entire drop freezes.

One method of modeling homogeneous freezing together with heterogeneous freezing is to fit an equation of drop freezing to laboratory data. This treatment is uncertain, because it assumes that the composition of a drop in the air is similar to that in a laboratory experiment, which is often performed with tap water. Thus, it is uncertain whether the experiments simulated heterogeneous or homogeneous freezing or both.

Several studies have suggested that the homogeneous–heterogeneous freezing (HHF) temperature is related logarithmically to drop volume (e.g., Bigg 1953; Vali 1971; Pitter and Pruppacher 1973). For heterogeneous freezing, this assumption is physical since IIN can be randomly distributed within a drop. Under this theory, the **fractional number of drops that freeze** at a given temperature and particle size is

$$F_{\mathrm{Fr},k,t} = \min\{\upsilon_{\mathrm{lq},k} \exp[-B\,(T_{\mathrm{c}} - T_{\mathrm{r}})]\,, 1\} \tag{18.65}$$

where $\upsilon_{\mathrm{lq},k}$ is the volume of a single liquid drop in bin k (cm^3), T_{c} is the temperature of a population of drops (°C), T_{r} is a reference temperature (°C), and B is a fitting coefficient ($^\circ\mathrm{C}^{-1}$). Since the equation is empirical, units do not equate. Equation (18.65) suggests that, the lower the temperature and the larger the single-particle volume, the greater the fractional number of drops that freeze. From the equation, the **equilibrium median freezing temperature** (°C), which is the temperature at which 50 percent of drops freeze ($F_{\mathrm{Fr}} = 0.5$), is

$$T_{\mathrm{mf}} = T_{\mathrm{r}} - \frac{1}{B}\ln\left(\frac{0.5}{\upsilon_{\mathrm{lq},k}}\right) \begin{cases} B = 0.475\,^\circ\mathrm{C}^{-1};\ T_{\mathrm{r}} = 0\,^\circ\mathrm{C} & T_m < -15\,^\circ\mathrm{C} \\ B = 1.85\,^\circ\mathrm{C}^{-1};\ T_{\mathrm{r}} = -11.14\,^\circ\mathrm{C} & -15\,^\circ\mathrm{C} \le T_m < -10\,^\circ\mathrm{C} \end{cases} \tag{18.66}$$

where the parameter values were derived in Jacobson (2003) from a fit to data of Pitter and Pruppacher (1973). Figure 18.8 compares the fits with the original data. The data suggest that the freezing rate follows logarithmically with drop volume only for temperatures below –15 °C. Above –10 °C, no drops freeze. Other values of B and T_{r} derived from laboratory data can be found in Danielsen *et al.* (1972) and Orville and Kopp (1977).

Example 18.5

Calculate the fraction of the number concentration of supercooled 10-μm- and 100-μm-radius liquid drops that freeze due to homogeneous-heterogeneous freezing at a temperature of −25 °C.

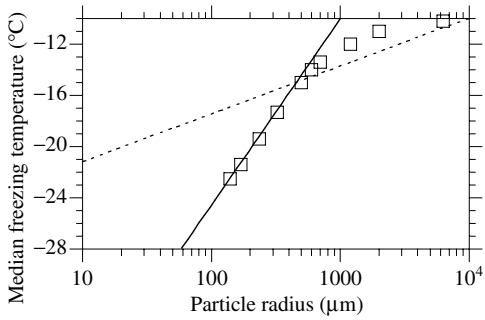

Figure 18.8 Comparison of fitted equation (18.66) for median freezing temperature with data of Pitter and Pruppacher (1973, Fig. 1), from which the fits were derived. From Jacobson (2003).

SOLUTION

From (18.65),

$$F_{\mathrm{Fr},10\mu\mathrm{m}} = 4.19 \times 10^{-9}\,\mathrm{cm}^3 \exp[-0.475\,^\circ\mathrm{C}^{-1}(-25\,^\circ\mathrm{C} - 0\,^\circ\mathrm{C})] = 0.000602$$

$$F_{\mathrm{Fr},100\mu\mathrm{m}} = 4.19 \times 10^{-6}\,\mathrm{cm}^3 \exp[-0.475\,^\circ\mathrm{C}^{-1}(-25\,^\circ\mathrm{C} - 0\,^\circ\mathrm{C})] = 0.602$$

Thus, a greater fraction of larger particles than smaller particles freeze at the same subfreezing temperature.

Equation (18.65) is an equilibrium equation. A **time-dependent freezing-rate** equation is

$$\frac{\mathrm{d}n_{\mathrm{gr},k,t}}{\mathrm{d}t} = n_{\mathrm{lq},k,t-h} v_{\mathrm{lq},k} A \exp[-B\,(T_\mathrm{c} - T_\mathrm{r})] \tag{18.67}$$

where $\mathrm{A} = 10^{-4}\mathrm{cm}^{-3}\mathrm{s}^{-1}$ (e.g., Orville and Kopp 1977; Reisin *et al.* 1996). Integrating this equation from $t = 0$ to h gives the **number concentration of liquid drops and graupel particles**, respectively, after homogeneous–heterogeneous freezing, as

$$n_{\mathrm{lq},k,t} = n_{\mathrm{lq},k,t-h}\,(1 - F_{\mathrm{Fr},k,t}) \tag{18.68}$$

$$n_{\mathrm{gr},k,t} = n_{\mathrm{gr},k,t-h} + n_{\mathrm{lq},k,t-h} F_{\mathrm{Fr},k,t} \tag{18.69}$$

where

$$F_{\mathrm{Fr},k,t} = 1 - \exp\{-h A v_{\mathrm{lq},k} \exp[-B(T_\mathrm{c} - T_\mathrm{r})]\} \tag{18.70}$$

is the **fractional number of drops that freeze.** Component volume concentrations are similarly calculated for liquid and graupel. Setting $F_{\mathrm{Fr},k,t} = 0.5$ and solving for

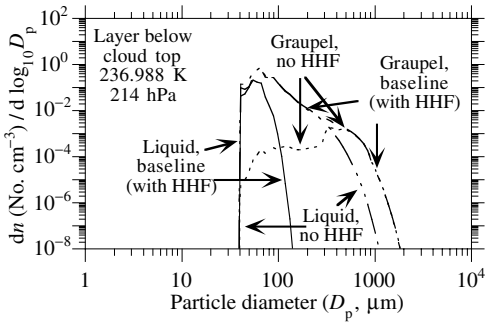

Figure 18.9 Comparison of modeled liquid and graupel distributions in the layer below cloud top from a simulation in which homogeneous-heterogeneous freezing (HHF) was calculated and one in which it was not. The time over which freezing occurred was one hour. The temperature is the initial in-cloud temperature. From Jacobson (2003).

T in (18.70) give the **time-dependent median freezing temperature** as

$$T_{\rm mf} = T_{\rm r} - \frac{1}{B}\ln\left(-\frac{\ln 0.5}{h A \upsilon_{{\rm lq},k}}\right) \tag{18.71}$$

Equating Equation (18.71) with (18.66) suggests that the time for equilibration is $h_{\rm eq} = -\ln 0.5/(0.5\,A) = 13\,862$ s when $A = 10^{-4}$ cm^{-3} s^{-1}. This time is much greater than the time step for typical atmospheric model processes.

Figure 18.9 illustrates the modeled effect on liquid and graupel size distributions of HHF over one hour. The figure shows that HHF (baseline case) converted primarily large liquid drops to graupel. The major effect of HHF was to increase 50–300 μm graupel particles. Since graupel in this size range merely replaces liquid, and because much of the graupel sublimates as it falls, the production of graupel due to HHF had little effect on hydrometeor or aerosol removal below the layer shown in the figure.

18.8.6 Drop surface temperature and evaporation/sublimation

When a hydrometeor particle falls below a cloud, where the air is subsaturated with respect to water vapor, the particle begins to evaporate or sublimate. The shrinkage rate of a small hydrometeor is sufficiently fast that the entire hydrometeor may dissipate to its aerosol-particle core. Large hydrometeors, though, often survive, possibly reaching the ground as rain or snow. Evaporation/sublimation reduces the surface temperature of a hydrometeor particle.

Here, equations are given to describe the final hydrometeor surface temperature and evaporation/sublimation rate when a hydrometeor falls through subsaturated

air. The procedure is performed by first calculating the equilibrium surface temperature iteratively then solving evaporation/sublimation using information from this information. This procedure is based on the method of Beard and Pruppacher (1971) and Pruppacher and Rasmussen (1979) with modification.

In the case of a liquid drop, the iteration involves solving the following equations:

$$
\begin{aligned}
p_{s,n} &= p_{v,s}(T_{s,n}) \\
\Delta p_{v,n} &= 0.3(p_{s,n} - p_{v,n}) \\
p_{f,n} &= 0.5(p_{s,n} + p_{v,n}) \\
T_{f,n} &= 0.5(T_{s,n} + T_a) \\
T_{s,n+1} &= T_{s,n} - \frac{D_v L_e}{\kappa_a (1 - p_{f,n}/p_a)} \frac{\Delta p_{v,n}}{R_v T_{f,n}} \\
p_{v,n+1} &= p_{v,n} + \Delta p_{v,n}
\end{aligned}
\tag{18.72}
$$

where the subscript n is the iteration number, $T_{s,n}$ is the **drop surface temperature** (K) at iteration n, initialized at the ambient temperature T_a (K), which stays constant, $p_{s,n}$ is the saturation vapor pressure (hPa) over the drop surface, evaluated at the drop surface temperature, $\Delta p_{v,n}$ is an estimated change in water vapor partial pressure at iteration n, $p_{f,n}$ and $T_{f,n}$ are average values of water vapor partial pressure and of temperature between the drop surface and ambient air, D_v is the diffusion coefficient of water vapor in air ($cm^2\ s^{-1}$), L_e is the latent heat of evaporation ($J\ g^{-1}$), κ_a is the thermal conductivity of moist air ($J\ cm^{-1}\ s^{-1}\ K^{-1}$), R_v is the gas constant for water vapor ($4614\ cm^3\ hPa\ g^{-1}\ K^{-1}$), and p_a is the ambient air pressure (hPa). The above set of equations is iterated a minimum of three times. The factor of 0.3 is included in $\Delta p_{v,n}$ to ensure convergence without overshooting.

The equations differ from Beard and Pruppacher (1971) only in that the present equations ignore ventilation coefficients for energy and vapor and radiative heating to eliminate the size-dependence of the iterative calculation, which would add to computer time without affecting the result significantly. For example, when size-dependent parameters are included, the difference in final drop surface temperature between a 0.001 and 1000 μm drop is only 2.5 percent (0.05 K/2 K) of the mean drop surface temperature depression when the relative humidity (RH) is 80 percent and the ambient temperature is 283.15 K. Even at RH = 1 percent, the difference is only 4 percent (0.4 K/10 K). Temperature equations for sublimation are analogous to those for evaporation.

Figure 18.10 shows the variation in equilibrium drop surface temperature and other parameters for initial relative humidities of 1 to 100 percent under (a) lower- (b) mid- and (c) upper-tropospheric conditions. The figure shows that, under lower-tropospheric conditions (Fig. 18.10(a)), drop surface temperatures can decrease by as much as 10 K when RH = 1 percent. At RH = 80 percent, which is more typical

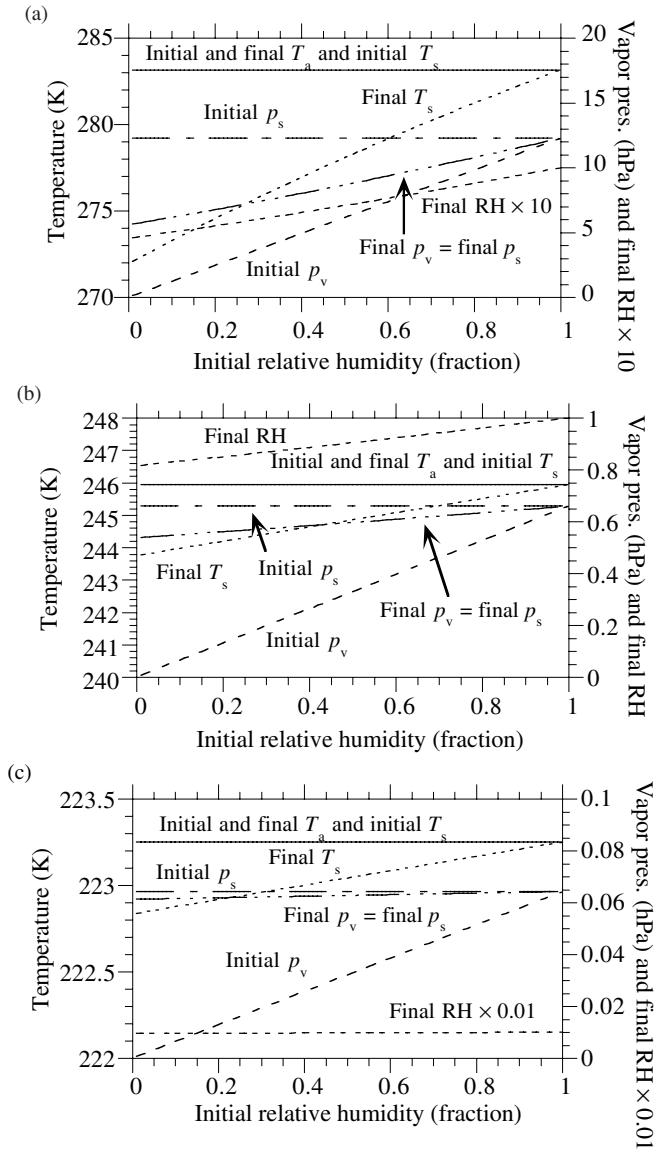

Figure 18.10 Variation in equilibrium liquid drop surface temperature (T_s, K), saturation vapor pressure over the drop surface (p_s, hPa), partial pressure of water away from the drop surface (p_v, hPa), and relative humidity (RH) near the drop surface for initial ambient relative humidities of 1 to 100 percent when (a) the ambient temperature (T_a) = 283.15 K and the air pressure (p_a) = 900 hPa (lower-tropospheric conditions), (b) T_a = 245.94 K and p_a = 440.7 hPa (middle-tropospheric conditions), and (c) T_a = 223.25 K and p_a = 265 hPa (upper-tropospheric conditions). The figure was obtained by solving Equation (18.72). From Jacobson (2003).

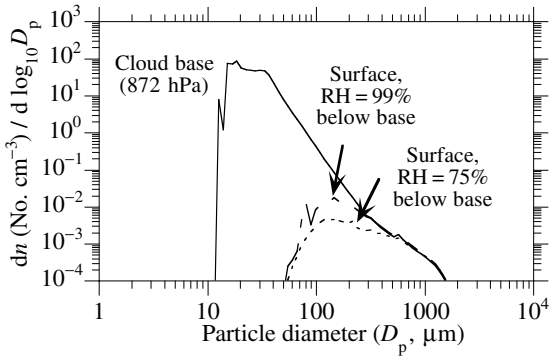

Figure 18.11 Effect of evaporation on the size distribution of precipitation drops reaching the surface after falling from a cloud base at about 1.25 km through subsaturated air in which the relative humidity (RH) was 99% and 75%, respectively. From Jacobson (2003).

below a cloud, the temperature depression is close to 2 K. Under mid-tropospheric conditions (Fig. 18.10(b)), supercooled drop temperatures can decrease by as much as 2.2 K when RH = 1 percent or 1 K when RH = 50 percent. Under upper-tropospheric conditions (Fig. 18.10(c)), the maximum temperature depression is about 0.5 K.

From the drop surface temperature and other parameters found iteratively, the change in drop liquid water volume concentration (cm^3 cm^{-3}) due to evaporation is

$$v_{\mathrm{L,lq},k,t,m} = \mathrm{MAX}\left[v_{\mathrm{L,lq},k,t-h} - \frac{n_{\mathrm{lq},k} 4\pi r_k D_\mathrm{v}}{(1 - p_{\mathrm{f},nf}/p_\mathrm{a})} \frac{(p_{\mathrm{v,s},0} - p_{\mathrm{v},nf})}{\rho_\mathrm{L} R_\mathrm{v} T_{\mathrm{f},nf}} \frac{\Delta z}{V_{\mathrm{f,lq},k}}, 0\right]_m \tag{18.73}$$

where the subscripts 0 and *nf* indicate initial and final iterated values, respectively, from (18.72), and the time step over which evaporation occurs is determined as the layer thickness (cm) divided by the fall speed (cm s^{-1}) ($\Delta z / V_{\mathrm{f,lq},k}$); thus it is the time that the hydrometeor can last in the layer before falling to the next layer. This time step is physical since, if the same time step were constant for all drop sizes, big drops with short lifetimes would evaporate for a longer period than they would last in the layer. The fall speed of a hydrometeor is discussed in Chapter 20. The sublimation rates of ice crystals falling through subsaturated air are calculated in a manner similar to those of liquid drops.

Figure 18.11 shows the modeled effect of evaporation on an idealized size distribution of liquid drops falling about 1.25 km from cloud base to the ground when the relative humidity is 99 percent and 75 percent. Evaporation eliminated almost all small drops in both cases and shrank drops more effectively at 75 percent than at 99 percent relative humidity.

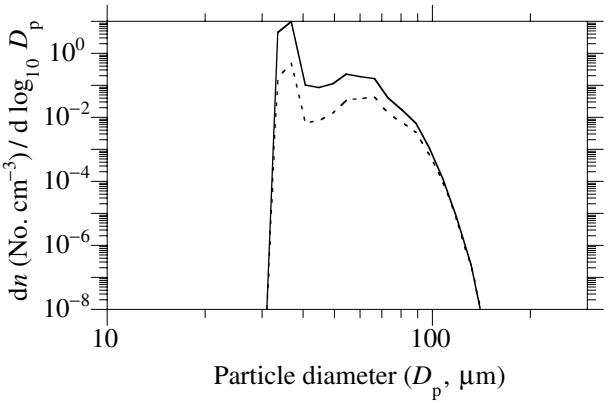

Figure 18.12 Incremental homogeneous-heterogeneous freezing due to evaporative cooling. The solid line (—) shows a liquid size distribution at an ambient pressure of 214 hPa, an ambient temperature of 236.988 K, and a relative humidity (RH) of 100%. When the RH decreases to 80%, the drop surface temperature decreases to 236.617 K, causing 5% more liquid drops to freeze by homogeneous-heterogeneous nucleation than would otherwise have frozen at 236.988 K. The incremental 5% is represented by the dashed line (----).

18.8.7 Evaporative freezing

As liquid drops falling through subsaturated air evaporate, their surfaces cool (Fig. 18.10). As temperatures decrease below $-10\,^{\circ}$C, the fractional number of liquid drops that freeze at a given size increases (Equation (18.65)). As such, the cooling of a liquid drop due to evaporation at its surface is a mechanism of drop freezing, termed **evaporative freezing** (Jacobson 2003). The initial temperature of freezing and the median freezing temperature of small drops are lower than are those of large drops, but even for small drops, evaporative cooling may enhance the probability of freezing under the right conditions.

Figure 18.12 illustrates evaporative freezing. The figure shows a liquid hydrometeor size distribution at a relative humidity of 100 percent and $T = 236.988$ K. Under these conditions, a portion of the distribution, determined from (18.65), freezes due to homogeneous-heterogeneous freezing. When the relative humidity drops to 80 percent, (18.72) predicts a decrease in the surface temperature of all drops by 0.35 K. At this lower temperature, (18.65) predicts an increase in the number concentration of drops that freeze by 5 percent. The dashed curve in Fig. 18.12 shows this incremental change in the number distribution of frozen drops due to evaporative freezing.

The theory that evaporative cooling at a drop's surface as the drop falls through subsaturated air may enhance its rate of freezing is analogous to the theory, shown experimentally by Rasmussen and Pruppacher (1982), that evaporative cooling delays the onset of melting.

The evaporative freezing theory also implies that homogeneous-heterogeneous drop freezing in subsaturated air may occur first on a drop surface rather than in the bulk of the drop. Homogeneous-heterogeneous freezing may also occur more readily at a drop surface than in the bulk of a drop for other reasons. Tabazadeh *et al.* (2002), for example, found that ice nucleation is thermodynamically favored on the surface in comparison with in the bulk of a liquid drop, even when no temperature gradient exists. Stuart (2002) found that, if a frozen nucleus forms in the middle of a drop, thin dendrites shoot out to the surface and warm the entire drop to the melting point within less than 0.1 s. Heat loss by the partially frozen drop occurs only by conduction and evaporation at the surface, causing the surface temperature to be cooler than the rest of the drop but warmer than the drop was originally. Due to the cooler surface relative to the interior, remaining freezing proceeds from the surface, inward. Thus, although freezing may initiate in the center, the rate of freezing quickly increases at the surface relative to the interior. The main difference between the mechanism of Stuart (2002) and pure evaporative freezing is that, with the former, surface freezing is triggered by freezing within the drop itself; with the latter, surface freezing is triggered by surface cooling as a drop falls through subsaturated air. Evaporative freezing can occur on its own or with one of these other mechanisms to enhance the rate of surface freezing.

18.8.8 Ice crystal melting

If the temperature of an ice crystal or graupel particle increases above the ice melting point (nominally $T_0 = 273.15$ K), the frozen hydrometeor begins to melt. But, when an ice crystal melts in subsaturated air (e.g., when the partial pressure of water away from the crystal surface is lower than the saturation vapor pressure over meltwater on the surface), simultaneous evaporation of the meltwater cools the particle surface, retarding the rate of melting. Thus, the melting temperature must exceed T_0 for the final drop surface temperature to equal T_0. The lower the relative humidity (partial pressure divided by saturation vapor pressure over liquid water), the greater the melting temperature.

The **melting point** of a population of ice particles can be found from

$$T_{\text{melt}} = T_0 + \text{MAX}\left\{\frac{D_v L_e}{\kappa_a R_v}\left[\frac{p_{v,s}(T_0)}{T_0} - \frac{p_v}{T_a}\right], 0\right\} \tag{18.74}$$

(Rasmussen and Pruppacher 1982), where $p_{v,s}(T_0)$ is the saturation vapor pressure over liquid water (hPa) at T_0, T_a is the ambient air temperature (K), p_v is the ambient partial pressure of water vapor (hPa), D_v is the diffusion coefficient of water vapor in air (cm^2 s^{-1}), L_e is the latent heat of evaporation (J g^{-1}), κ_a is the thermal conductivity of moist air (J cm^{-1} s^{-1} K^{-1}), and R_v is the gas constant for water vapor (4614 cm^3 hPa g^{-1} K^{-1}). When melting occurs, the change in mass (g)

of ice in a particle of a given size is

$$m_{\mathrm{ic},Ni,t} = m_{\mathrm{ic},Ni,t-h} - \mathrm{MAX}\left\{h\frac{4\pi r_{Ni}}{L_\mathrm{m}}\left[\kappa_\mathrm{a}\left(T_\mathrm{a}-T_0\right)F_{h,\mathrm{I},Ni} - \frac{D_\mathrm{v}L_\mathrm{e}}{R_\mathrm{v}}\left(\frac{p_{\mathrm{v,s}}\left(T_0\right)}{T_0}-\frac{p_\mathrm{v}}{\mathrm{T_a}}\right)F_{\mathrm{v,I},Ni}\right], 0\right\} \tag{18.75}$$

(e.g., Rasmussen *et al.* 1984), where L_m is the latent heat of melting (J g^{-1}) and h is the time step (s). Although the rate of melting increases linearly with increasing particle radius, mass increases with radius cubed, so small crystals melt completely much faster than do large crystals.

Example 18.6

Calculate the melting temperature of a frozen particle when the ambient temperature is 273.15 K, total air pressure is 970 hPa, and the relative humidity is 80 percent.

SOLUTION

From (8.14), the diffusion coefficient of water vapor in air is $D_\mathrm{v} = 2.204 \times 10^{-5}$ m^2 s^{-1}. From (2.62), the saturation vapor pressure at 273.15 K is $p_{\mathrm{s,v}} = 6.112$ hPa. From (2.66), the partial pressure of water vapor at a relative humidity of 80 percent and at 273.15 K is $p_\mathrm{v} = 4.89$ hPa. From (2.54), the latent heat of evaporation at 273.15 K is $L_\mathrm{e} = 2.501 \times 10^6$ J kg^{-1}. From (2.5) and (2.6), the thermal conductivities of dry air and water vapor are $\kappa_\mathrm{d} = 0.023807$ and $\kappa_\mathrm{v} = 0.015606$ J m^{-1} s^{-1} K^{-1}, respectively, at 273.15 K. Since $n_\mathrm{v}/(n_\mathrm{v}+n_\mathrm{d}) = p_\mathrm{v}/p_\mathrm{a}$, the thermal conductivity of moist air from (2.7) is then $\kappa_\mathrm{a} = 0.023746$ J m^{-1} s^{-1} K^{-1}. Substituting these values into (18.74) gives the melting point of an ice crystal as

$$T_\mathrm{melt} = 273.15\,\mathrm{K} + \frac{2.204\times10^{-5}\,\dfrac{\mathrm{m}^2}{\mathrm{s}}\times 2.501\times10^{6}\,\dfrac{\mathrm{J}}{\mathrm{kg}}}{0.023746\,\dfrac{\mathrm{J}}{\mathrm{m\,s\,K}}\times 461.4\,\dfrac{\mathrm{J}}{\mathrm{kg\,K}}} \times\left[\frac{6.112\,\mathrm{hPa}}{273.15\,\mathrm{K}}-\frac{4.89\,\mathrm{hPa}}{273.15\,\mathrm{K}}\right]\frac{100\,\mathrm{J}}{\mathrm{hPa\,m}^3} = 275.40\,\mathrm{K}$$

Thus, the melting point of an ice crystal at 80 percent relative humidity is greater than that at 100 percent relative humidity.

18.8.9 Aerosol–hydrometeor coagulation: aerosol washout

The two major mechanisms of aerosol removal by precipitation are **nucleation scavenging** (rainout) and **aerosol–hydrometeor coagulation** (washout). **Rainout** occurs when a CCN activates to form a liquid drop, and the drop coagulates with other drops to become rain or graupel, which falls to the surface, removing the

CCN inclusions. **Washout** occurs when growing or falling precipitation particles coagulate with interstitial aerosol particles and fall to the surface, bringing the aerosol particles with them.

Together, rainout and washout are the most important mechanisms removing aerosol particles globally. The other mechanisms of aerosol removal, gravitational settling and dry deposition, are important for very large particles and over long periods, but not so important relative to rainout and washout for small particles over short periods.

Aerosol–hydrometeor coagulation results in the coalescence of aerosol particles with liquid or frozen hydrometeors, reducing aerosol particle number. The final aerosol-particle total volume concentration ($x = T$), solution volume concentration ($x = s$), or individual component concentration ($x = q$) in bin k of aerosol distribution N after one time step of aerosol–hydrometeor coagulation can be calculated as

$$\upsilon_{x,Nk,t} = \frac{\upsilon_{x,Nk,t-h}}{1 + hT_{x,Nk,t,3}}$$

$$T_{x,Nk,t,3} = \sum_{j=1}^{N_C} \left[\sum_{M=1}^{N_H} \beta_{Nk,Mj,t-h} n_{Mj,t-h} \right] \tag{18.76}$$

where N_H is the total number of hydrometeor distributions and N_C is the number of bins in each hydrometeor distribution. Equation (18.76) is solved for all aerosol distributions $N = 1 \ldots N_T$ and size bins $k = 1 \ldots N_B$ per distribution. The corresponding final volume concentrations of hydrometeor particles and their aerosol inclusions within size bin k of hydrometeor distribution Y after one time step is

$$\upsilon_{x,Yk,t} = \frac{\upsilon_{x,Yk,t-h} + h\left(T_{x,Yk,t,1} + T_{x,Yk,t,2}\right)}{1 + hT_{x,Yk,t,3}}$$

$$T_{x,Yk,t,1} = \sum_{N=1}^{N_T} \left[\sum_{j=1}^{k} \left(n_{Nj,t-h} \sum_{i=1}^{k-1} f_{Yi,Nj,Yk} \beta_{Yi,Nj,t-h} \upsilon_{x,Yi,t} \right) \right]$$

$$T_{x,Yk,t,2} = \sum_{N=1}^{N_T} \left[\sum_{j=1}^{k} \left(n_{Yj,t-h} \sum_{i=1}^{k} f_{Ni,Yj,Yk} \beta_{Ni,Yj,t-h} \upsilon_{x,Ni,t} \right) \right]$$

$$T_{x,Yk,t,3} = \sum_{j=1}^{N_B} \left[\sum_{N=1}^{N_T} (1 - f_{Yk,Nj,Yk}) \beta_{Yk,Nj,t-h} n_{Nj,t-h} \right] \tag{18.77}$$

which is solved for all hydrometeor distributions $Y = 1 \ldots N_H$ and size bins $k = 1 \ldots N_C$. The volume fractions (e.g., $f_{Yi,Nj,Yk}$) in (18.77) are calculated in the same manner as in (18.55) but, here, represent the fraction of a coagulated hydrometeor–aerosol particle partitioned into a hydrometeor bin. The final number concentrations of aerosol particles and hydrometeor particles following aerosol–hydrometeor coagulation are

$$n_{Nk,t} = \frac{\upsilon_{T,Nk,t}}{\upsilon_{Nk}} \qquad N = 1 \ldots N_T;\ k = 1 \ldots N_B \tag{18.78}$$

$$n_{Yk,t} = \frac{\upsilon_{T,Yk,t}}{\upsilon_{Yk}} \qquad Y = 1 \ldots N_H;\ k = 1 \ldots N_C \tag{18.79}$$

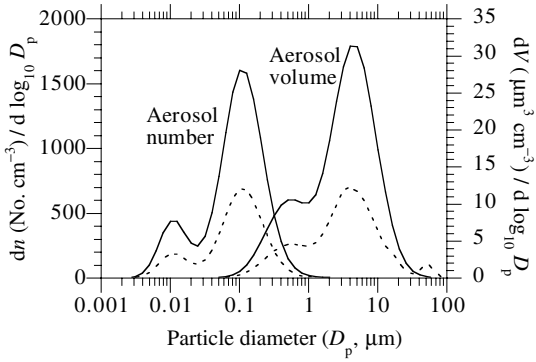

Figure 18.13 Below-cloud-base aerosol number and volume concentration (at 902 hpa), summed over 16 size distributions, before (solid lines) and after (short-dashed lines) aerosol–hydrometeor coagulation. The simulation period was one hour.

respectively. The scheme described above is volume and volume-concentration conserving, positive definite, and noniterative. Aerosol–hydrometeor coagulation kernels are given in Section 15.6.

Within a cloud, rainout removes >50 percent, whereas washout removes <0.1 percent of aerosol mass (e.g., Kreidenweis *et al.* 1997; Jacobson 2003). Rainout scavenges all large and most midsize particles, which have large mass, before washout has a chance to remove particles within a cloud. Within a cloud, rainout may remove 30 to >50% of aerosol number (e.g., Flossmann *et al.* 1985; Jacobson 2003; Kreidenweis *et al.* 2003). However, below a cloud, rainout does not remove aerosol particles since no activation of new drops occurs below a cloud. Thus, all below-cloud removal of aerosol particles is by washout. Figure 18.13 shows the modeled effect of below-cloud washout on the size distribution of aerosol particles. Washout removed aerosol particles across the entire size distribution. Because washout removes small particles within a cloud (large particles in a cloud are removed by rainout) and washout removes small and large particles below a cloud, washout generally removes more particles within plus below cloud by number than does rainout (Jacobson 2003).

18.8.10 Gas washout

Precipitation removes soluble gases by washout. As a raindrop falls through air containing a soluble gas, the gas may dissolve in the drop. As the drop falls further, more gas will dissolve if the air is supersaturated with the gas (i.e., if the partial pressure of the gas exceeds its saturation vapor pressure as determined by the molality of the dissolved gas in rainwater divided by its Henry's law constant). If the air is undersaturated some of the gas in the drop will evaporate to maintain saturation at the drop surface. To complicate matters, a gas may dissolve in drops of one size and evaporate from drops of a different size in a layer.

Below, a parameterization for gas washout is given. It accounts for the changing amount of solute, summed over drops of all sizes, as the drops fall through the air. The numerical solution is derived by considering the **gas–hydrometeor equilibrium relation,**

$$\frac{c_{q,\mathrm{lq},t,m}}{C_{q,t,m}} = H'_q R^* T \sum_{k=1}^{N_C} p_{L,\mathrm{lq},t,k,m} \tag{18.80}$$

and the **gas–hydrometeor mole-balance equation**

$$C_{q,t,m} + c_{q,\mathrm{lq},t,m} = C_{q,t-h,m} + c_{q,\mathrm{lq},t,m-1} \frac{\Delta z_{m-1}}{\Delta z_m} \tag{18.81}$$

where m is the layer of the model atmosphere (increasing from 1 at the top to the number of model layers), Δz_m is the thickness (cm) of a layer, $C_{q,t,m}$ is the mole concentration of gas q (mol cm^{-3}), $c_{q,\mathrm{lq},t,m}$ is the mole concentration of the dissolved gas, summed over all size bins $k = 1 \ldots N_C$ in the liquid hydrometeor size distribution, $p_{L,\mathrm{lq},t,k,m}$ is liquid precipitation passing through layer m in bin k (cm^3 cm^{-3}), R^* is the ideal gas constant (0.08206 L atm mol^{-1} K^{-1}), H'_q is an effective Henry's constant for species q (mol L^{-1} atm^{-1}), and T is temperature (K). Equation (18.81) states that the final gas plus aqueous species concentration after dissolution/evaporation equals the initial gas concentration in the layer plus the aqueous concentration in precipitation from the layer above. For the top cloud layer, $c_{q,\mathrm{lq},t,m-1} = 0$. Combining (18.80) and (18.81) gives the **final gas concentration** in any layer m as

$$C_{q,t,m} = \frac{C_{q,t-h,m} + c_{q,\mathrm{lq},t,m-1} \dfrac{\Delta z_{m-1}}{\Delta z_m}}{1 + H'_q R^* T \displaystyle\sum_{k=1}^{N_C} p_{L,\mathrm{lq},t,m}} \tag{18.82}$$

The **final aqueous mole concentration,** used for the calculation in the next layer, is

$$c_{q,\mathrm{lq},t,m} = C_{q,t-h,m} + c_{q,\mathrm{lq},t,m-1} \frac{\Delta z_{m-1}}{\Delta z_m} - C_{q,t,m} \tag{18.83}$$

This solution is exactly mole conserving, noniterative, unconditionally stable, and positive definite. It states that if rainwater passing through a model layer is already saturated with dissolved gas (the air is saturated or undersaturated with the gas), no additional gas can enter the rainwater, but some may evaporate in the current layer. This mechanism not only removes gases but also transfers gases from a supersaturated layer to a subsaturated layer. The formulation given here applies ideally to soluble gases that are not chemically reactive in solution. For reactive gases, particularly SO_2, aqueous chemical reactions often occur on time scales shorter than the time a drop takes to fall from one layer to the next. Irreversible aqueous chemical reactions occurring within drops are discussed in Chapter 19.

18.8.11 Lightning

Lightning is a bolt of electricity that travels between two regions of a cloud, between two clouds, or between a cloud and the ground. A lightning stroke heats the air to greater than 30 000 °C. The heating causes the air to expand violently, creating a shock wave that propagates at the speed of sound (about 330 m s^{-1}), producing **thunder**. The energy of the lightning bolt is also intense enough to split molecular nitrogen (N_2) and molecular oxygen (O_2) to N and O, respectively, which together react to form nitric oxide (NO). Thus, lightning is a natural source of NO in the atmosphere.

Lightning occurs following the buildup of opposite charges between one part of a cloud and either another part of the same cloud, a part of another cloud, or the ground. The opposing charges create an attractive electrostatic force that becomes strong enough to cause a discharge in electricity.

The force (N) between two point charges Q_0 (C) and Q_1 (C) separated by distance r_{01} (m) is called the **electrostatic force** and is determined by **Coulomb's law**,

$$F_e = \frac{k_C Q_0 Q_1}{r_{01}^2} \tag{18.84}$$

which states that the force between two point charges varies inversely as the square of the distance separating the charges and is proportional to the magnitude of each charge. The force is attractive if the point charges have opposite sign. It is repulsive if they have the same sign. The constant in the equation is **Coulomb's constant**,

$$k_C = \frac{1}{4\pi\varepsilon_0} = 8.98755 \times 10^9 \,\mathrm{N\,m^2\,C^{-2}} = 8.98755 \times 10^{11} \,\mathrm{V\,cm\,C^{-1}} \tag{18.85}$$

which is measured experimentally and is usually written in terms of the **permittivity of free space**, $\varepsilon_0 = 8.85419 \times 10^{-12}$ $\mathrm{C^2\,N^{-1}\,m^{-2}} = 8.85419 \times 10^{-14}$ $\mathrm{C\,V^{-1}\,cm^{-1}}$, where 1 V = 1 J C^{-1} and 1 J = 1 N m. The smallest possible charge is that on an electron, $Q = 1.6 \times 10^{-19}$ C.

The **electric field strength** is defined for a specific location as the sum of electrostatic forces between a point charge at that location and point charges at all surrounding locations, divided by the charge at the location of interest. For example, the electric field strength at the location of charge Q_0 due to forces between Q_0 and all charges Q_i separated by distance r_{0i} is

$$E_f = \sum_i \frac{F_{e,0i}}{Q_0} = \sum_i \frac{k_C Q_i}{r_{0i}^2} \tag{18.86}$$

which has units of N C^{-1} (V m^{-1}).

Lightning occurs only when the electric field strength exceeds the **threshold electric field strength**, E_{th}, which ranges from 100 to 400 kV m^{-1}, with an average of 300 kV m^{-1}. In the absence of clouds, the upper atmosphere is charged slightly

positive and the surface of the Earth is charged slightly negative, resulting in an electric field strength near the surface of only about 130 V m^{-1}. The average charge density at the ground is about 21 electrons cm^{-3}. The charge density averaged in the first kilometer above the ground is about 5 electrons cm^{-3} (Pruppacher and Klett 1997).

One theory of how clouds become electrified enough for lightning to form is the theory of **particle rebound charging**. According to this theory, large liquid drops, ice crystals, and graupel particles that are polarized with a net negative charge on their top and positive charge on their bottom may become negatively charged overall when they collide with and bounce off smaller liquid or ice hydrometeors that are also polarized. Since large particles fall faster than small particles, a falling large particle, which has a positive charge, is hit on its bottom by a small particle in its path. During the brief collision, the positive charge from the bottom of the large particle transfers to the small particle, giving the large particle a net negative charge and the small one a net positive charge. Since the large particle is heavy, it continues falling toward the bottom of the cloud whereas the small particle, which is light, stays suspended near the middle or top of the cloud.

Rebound charging can be enhanced by the **thermo-electric effect**. As graupel and hail fall through the air, they grow by collision and coalescence with supercooled liquid water drops, which freeze upon contact. The release of latent heat due to the freezing warms the surface of the graupel or hail. When these warm hydrometeor particles subsequently collide with and bounce off smaller ice crystals, a net transfer of positively charged hydrogen ions (H^+) occurs from the warmer graupel and hail to the colder crystals. Negatively charged OH^- ions try to diffuse in the opposite direction, but their mobility is lower than that of H^+ ions.

As a thunderstorm cloud gains strength, the charge differential between its top and base grows, due in part to the thermo-electric rebound charging mechanism, and intracloud lightning may occur. Since the cloud base is now predominantly negatively charged, it induces a positive charge on the Earth's surface, which is normally slightly negatively charged. If the charge difference between the cloud base and ground increases above the threshold electric field strength, cloud-to-ground lightning occurs. Several other possible cloud charging mechanisms are described in Pruppacher and Klett (1997).

Lightning generation by the **rebound charging mechanism** can be modeled by considering the collision and bounceoff of size-resolved liquid and solid hydrometeors. The **rate coefficient for bounceoff** (bounceoff kernel) (cm^3 $particle^{-1}$ s^{-1}) of a particle in size bin i of hydrometeor distribution I interacting with a particle in size bin j of hydrometeor distribution J in any model layer m of a cloud is

$$B_{Ii,Jj,m} = (1 - E_{\text{coal},Ii,Jj,m}) K_{Ii,Jj,m} \tag{18.87}$$

where $E_{\text{coal},Ii,Jj,m}$ is the dimensionless coalescence efficiency, discussed in Section 15.6.8, and $K_{Ii,Jj,m}$ is the collision kernel (cm^3 $particle^{-1}$ s^{-1}) discussed in Section 15.6. Combining the bounceoff kernel with other terms gives the **charge separation**

rate per unit volume of air (C cm^{-3} s^{-1}) in layer m,

$$\frac{\mathrm{d}Q_{b,m}}{\mathrm{d}t} = \left[\sum_{J=2}^{N_\mathrm{H}}\sum_{j=1}^{N_\mathrm{C}}\sum_{I=J}^{N_\mathrm{H}}\sum_{i=j}^{N_\mathrm{C}} B_{Ii,Jj}\frac{(\upsilon_{Ii}n_{Ii,t}n_{Jj,t-b} + \upsilon_{Jj}n_{Ii,t-b}n_{Jj,t})}{\upsilon_{Ii}+\upsilon_{Jj}}\Delta Q_{Ii,Jj}\right]_m \tag{18.88}$$

where N_H is the number of hydrometeor distributions, n is the number concentration of hydrometeor particles (particles cm^{-3}), υ is the volume of a single particle (cm^3 particle^{-1}), and $\Delta Q_{Ii,Jj}$ is the **charge separation per collision** (coulombs per collision). The charge separation per bounceoff due to the thermo-electric rebound charging mechanism is in the range $1-5 \times 10^{-14}$ C per collision, with an average of 3.33×10^{-14} C per collision (Pruppacher and Klett 1997). The charge separated during a collision is a complex function of the available charge on each colliding particle, the angle and surface area of collision, the time during which contact occurs, and the temperature. The charge separation (C per collision), though, must be limited by

$$\Delta Q_{Ii,Jj} = \min[3.33 \times 10^{-16}\,\mathrm{C}, 0.5(Q_{Ii} + Q_{Jj})] \tag{18.89}$$

where

$$Q_{Ii} = 3.333 \times 10^{-10} \times 2r_{Ii}^2 \tag{18.90}$$

(and a similar expression for Q_{Jj}) is the total charge (C) on a single particle in a highly electrified, precipitating cloud from (15.63), where r_{Ii} is the radius in cm.

In the equations discussed in this chapter, $N_\mathrm{H} = 3$, where distributions 1–3 are liquid, ice, and graupel distributions, respectively. Since the thermo-electric rebound charging mechanism occurs among ice crystals and graupel, the first summation in (18.88) considers interactions among only distributions 2 and 3. Thus, (18.88) treats bounceoffs during size-resolved ice–ice, ice–graupel, and graupel–graupel interactions.

Summing the charge separation rate from (18.88) over all cloud layers and multiplying the result by the cloudy-sky area of the model column give the **overall charge separation rate** in the cloudy region of a model column as

$$\frac{\mathrm{d}Q_{\mathrm{b,c}}}{\mathrm{d}t} = F_\mathrm{c}A_\mathrm{cell}\sum_{m=K_\mathrm{top}}^{K_\mathrm{bot}}\frac{\mathrm{d}Q_{\mathrm{b},m}}{\mathrm{d}t}\Delta z_m \tag{18.91}$$

(C s^{-1}) where F_c is the cloud fraction in a model column, A_cell is the total horizontal area of the grid cell (cm^2), and Δz_m is the vertical thickness of each model layer (cm).

The overall charge separation rate is used to calculate the **time-rate-of-change of the in-cloud electric-field strength** (V cm^{-1} s^{-1}),

$$\frac{\mathrm{d}E_\mathrm{f}}{\mathrm{d}t} = \frac{2k_\mathrm{C}}{Z_\mathrm{c}\sqrt{Z_\mathrm{c}^2 + R_\mathrm{c}^2}}\frac{\mathrm{d}Q_{\mathrm{b,c}}}{\mathrm{d}t} \tag{18.92}$$

(e.g., Wang and Prinn 2000), where E_f is in units of V cm^{-1}, k_C is Coulomb's constant from (18.85),

$$Z_c = \sum_{m=K_{top}}^{K_{bot}} \Delta z_m \tag{18.93}$$

is the **summed vertical thickness of cloud layers** between the bottom layer (K_{bot}) and top layer (K_{top}) of the cloud (cm), and

$$R_c = \sqrt{F_c A_{cell}/\pi} \tag{18.94}$$

is the **horizontal radius of the cloudy region** (cm).

The number of intracloud flashes per centimeter per second can now be estimated with

$$\frac{dF_r}{dt} = \frac{1}{Z_c E_{th}} \frac{dE_f}{dt} \tag{18.95}$$

where F_r is the number of flashes per centimeter and E_{th} is the **threshold electric field strength** (V cm^{-1}) defined previously. The cloud-to-ground flash rate is approximately 30–45 percent of the intracloud flashrate (Price *et al.* 1997; Boccippio *et al.* 2001).

Example 18.7

Calculate the number of flashes per hour in a cylindrical cloud of radius 0.5 km and thickness 5 km when two populations of particles, with number concentrations 1000 and 0.05 particles cm^{-3}, respectively, are present. Assume the collision kernel between the populations is 10^{-4} cm^3 particle^{-1} s^{-1} and that the coalescence efficiency is 40 percent.

SOLUTION

The charge separation rate for this problem is

$$\begin{aligned}\frac{dQ_{b,c}}{dt} &= B_{1,2} n_1 n_2 \Delta Q_{1,2} V_c \\ &= (1 - 0.4) \times 10^{-4} \frac{\text{cm}^3}{\text{partic. s}} \times \frac{1000 \text{ partic.}}{\text{cm}^3} \times \frac{0.05 \text{ partic.}}{\text{cm}^3} \\ &\quad \times \frac{3.33 \times 10^{-14} \text{ C}}{\text{collision}} \times 1.25 \times 10^{15} \text{ cm}^3 = 0.125 \frac{\text{C}}{\text{s}}\end{aligned}$$

where $V_c = 1.25 \times 10^{15}$ cm^3 is the volume of the cylindrical cloud. From (18.92), the rate of change of the in-cloud electric field strength is

$$\frac{dE_f}{dt} = \frac{2 \times 8.98755 \times 10^{11} \frac{\text{V cm}}{\text{C}}}{5 \times 10^5 \text{ cm} \sqrt{(5 \times 10^5 \text{ cm})^2 + (0.5 \times 10^5 \text{ cm})^2}} \times 0.125 \frac{\text{C}}{\text{s}} = 0.894 \frac{\text{V}}{\text{cm s}}$$

The number of intracloud flashes per hour in the cloud is then

$$\frac{1}{E_{\text{th}}}\frac{\mathrm{d}E_{\text{f}}}{\mathrm{d}t} = \frac{1}{3000\dfrac{\text{V}}{\text{cm flash}}}\,0.894\,\frac{\text{V}}{\text{cms}} = 2.98\times10^{-4}\,\frac{\text{flashes}}{\text{s}} = 1.07\,\frac{\text{flashes}}{\text{hr}}$$

Finally, the **number of nitric oxide (NO) molecules produced per cubic centimeter of air per second** within a lightning region of a cloud or between the cloud and the ground is

$$E_{\text{NO}} = \frac{E_{\text{l}}F_{\text{NO}}}{A_{\text{cell}}}\frac{\mathrm{d}F_{\text{r}}}{\mathrm{d}t} \tag{18.96}$$

where E_{l} is the **number of joules per lightning flash** and F_{NO} is the **number of NO molecules produced per joule** of energy released. Values of E_{l} for cloud-to-ground lightning range from 1.8 to 11 GJ/flash with a mean of 6.7 GJ/flash (Price *et al.* 1997). The energy released by intracloud lightning is about 10 percent that of cloud-to-ground lightning. Values of F_{NO} are in the range $5–15\times10^{16}$ molecules NO/J with an average of 10^{17} molecules NO/J (Price *et al.* 1997). These values give the **number of NO molecules per flash** as $9\times10^{25}–1.7\times10^{27}$ for cloud-to-ground lightning and $9\times10^{24}–1.7\times10^{26}$ for intracloud lightning. An observed NO production rate for intracloud lightning is 2.6×10^{25} molecules NO/flash (Skamarock *et al.* 2003). Estimates of the total NO produced by lightning range from 5 to 20 Tg-N per year (Price *et al.* 1997; Bond *et al.* 2002).

18.9 SUMMARY

In this chapter, cloud, fog, and precipitation classification, formation, development, microphysics, and interactions with aerosol particles were discussed. Clouds form by free convection, orographic uplifting, forced convection, and lifting along frontal boundaries. Fogs form by radiational cooling, advection of warm moist air over a cool surface, orographic uplifting, and evaporation of warm water into cold air. When air rises in a cloud, it expands and cools pseudoadiabatically. Condensation adds energy and buoyancy to a cloud, and entrainment of outside air causes cooling and downdrafts along its edges. The thermodynamic energy equation for a cloud takes account of convection, latent-heat release, entrainment, and radiative effects. Due to strong inertial accelerations in a cloud, the hydrostatic approximation is not valid; thus, a vertical momentum equation with an inertial acceleration term is needed. Microphysical processes affecting cloud evolution include condensation/deposition, coagulation, drop breakup, contact freezing, homogeneous-heterogeneous freezing, evaporative freezing, evaporation/sublimation, and melting. Aerosol particles are removed by clouds and precipitation through rainout (nucleation scavenging) and washout (aerosol–hydrometeor coagulation). Gases are removed by gas washout. Collision followed by bounceoff among frozen

hydrometeors results in charge separation that can produce lightning, a major natural source of nitric oxide in the atmosphere.

18.10 PROBLEMS

18.1 Calculate the pseudoadiabatic lapse rate when $p_d = 900$ hPa and $T = 273.15$ K.

18.2 Calculate the dew-point lapse rate in an unsaturated parcel of air that rises from $p_d = 1000$ hPa to $p_d = 900$ hPa. Assume $\omega_v = 0.003$ kg kg^{-1} and does not change in the parcel, and the average $T_v = 279$ K.

18.3 Calculate the critical radius and critical supersaturation when a population of 1500 particles cm^{-3}, all with radius of 0.1 μm, contains 1×10^{-16} mol cm^{-3}-air of an organic compound that does not dissociate. Assume $T = 298.15$ K.

18.4 Calculate the median freezing temperature of a liquid water drop of radius (a) 10 μm and (b) 1000 μm. At which size does a higher fraction of drops freeze at a constant temperature?

18.5 Explain the difference between contact freezing and heterogeneous freezing.

18.6 Calculate the time required for 40 percent of liquid drops to contact freeze in the presence of 1000 aerosol particles cm^{-3} if the temperature is $-15\,^{\circ}$C, the coagulation rate coefficient is 10^{-4} cm^3 particle^{-1} s^{-1}, and a maximum of 5 percent of the aerosol particles present can serve as contact nuclei.

18.7 Calculate the melting temperature of a frozen particle when the ambient temperature is 298.15 K, total air pressure is 1013.25 hPa, and the relative humidity is 50 percent.

18.8 **(a)** If the number concentrations of particles 10 and 100 μm in radius are 1000 and 0.1 particles cm^{-3}, respectively, the collision kernel between particles of these two sizes is 10^{-5} cm^3 particle^{-1} s^{-1}, and the coalescence efficiency is 30 percent, calculate the number of lightning flashes after one hour in a cloud column 1 km thick and 1 km in radius. Assume the charge separation per bounceoff is 3.33×10^{-16} C and the threshold electric field strength is 300 kV m^{-1}.

(b) What is the average number concentration of NO molecules resulting from the lightning after one hour assuming no molecules existed initially?

18.11 COMPUTER PROGRAMMING PRACTICE

18.9 Write a computer script to calculate the pseudoadiabatic lapse rate between $z = 0$ and 10 km. Assume $T = 288$ K at the surface and decreases 6.5 K km^{-1} and the air is saturated with water vapor. Assuming $p_a = 1013.25$ hPa at the surface, use (2.44) to estimate p_a at each subsequent altitude. Use the program to estimate the pseudoadiabatic lapse rate at 100-m increments.

18.10 Assume that, at the surface, $T = 285$ K, $T_D = 278$ K, $p_a = 998$ hPa, and $\partial T/\partial z = -11$ K km^{-1}. Write a computer script to estimate p_a and T at the lifting

condensation level. [Hint: First estimate p_v at the surface from (2.68), which gives $p_d = p_a - p_v$, then use the result to obtain ω_v which stays constant in the rising parcel of air. Estimate the decrease in p_a with altitude from (2.42). Use ω_v and p_d to estimate T_D at each altitude.]

18.11 Write a computer code to calculate the total number of drops, integrated over all sizes, that result from the breakup of one 5-mm diameter liquid water drop assuming the breakup distribution from (18.57). Use a volume ratio size distribution with 100 size bins between 10 and 5500 μm.

18.12 Write a computer program to replicate Fig. 18.10(a).